NASA CR-112104

EVALUATION OF ADVANCED COMPONENT CONCEPTS FOR AN INTEGRATED ENVIRONMENTAL CONTROL/LIFE SUPPORT RESISTOJET CONTROL SYSTEM

By Carl R. Halbach, Paul D. Arthur,
and Russell J. Page

JUNE 1972

Prepared under Contract No. NAS1-10767 by

ADVANCED ROCKET TECHNOLOGY (ARTCOR)

Irvine, California 92664

for

NATIONAL AERONAUTICS AND SPACE ADMINISTRATION

Langley Research Center

EVALUATION OF ADVANCED COMPONENT CONCEPTS FOR AN INTEGRATED ENVIRONMENTAL CONTROL/ LIFE SUPPORT - RESISTOJET CONTROL SYSTEM

By Carl R. Halbach, Paul D. Arthur, and Russell J. Page

June 1972

Prepared under Contract No. NAS1-10767 by
ADVANCED ROCKET TECHNOLOGY (ARTCOR)
Irvine, California

for

NATIONAL AERONAUTICS AND SPACE ADMINISTRATION

Langley Research Center

TABLE OF CONTENTS

LIST OF FIGURES

LIST OF TABLES

EVALUATION OF ADVANCED COMPONENT CONCEPTS FOR AN INTEGRATED ENVIRONMENTAL CONTROL/ LIFE SUPPORT - RESISTOJET CONTROL SYSTEM

By Carl R. Halbach, Paul D. Arthur*, and Russell J. Page

Advanced Rocket Technology (ARTCOR)
Irvine, California

SUMMARY

Flow restricting devices have been studied for their suitability as liquid water propellant flow limiters for the biowaste resistojet. Flow limiting during the start-up transient is required to prevent thrustor instabilities and icing which could result in heater failure in the electrical resistance heated thrustor (resistojet). The study was directed toward simple devices which would function passively (i.e., without power except from the propellant flow itself), and would offer high reliability and simplicity.

A pre-evaporator (referred to simply as an evaporator) used in conjunction with the biowaste resistojet can serve as a relatively effective flow limiter by itself. To perform this function, however, the evaporator must have sufficient size (thermal capacity), and it must be preheated before propellant flow is commanded on. Significant improvement in thrustor flow stability can be provided by employing a flow restrictor such as an orifice, preferably used in conjunction with an evaporator to minimize thermal shock in the thrustor itself. With the use of a flow restrictor, the evaporator can be made smaller and lighter and the preheat time can be significantly shortened. Perfect flow limiting (constant mass flow rate) is not necessarily desired. Optimum thrustor response would normally occur with a slightly higher initial mass flow. The optimum flow limiter - evaporator - thrustor combination depends on the thrustor size, power available, and application requirements.

An orifice or nozzle restrictor was found to provide good flow limiting performance by limiting the initial mass flow rate to about 1.8 times the final steady-state value. A hybrid device has been demonstrated with improved flow limiting capability relative to the orifice or nozzle. For the same typical conditions, an initial-to-final mass flow ratio of about 1.2 is possible. The device utilizes a stiff diaphragm flexing through a short distance to cover one of two orifices. As pressure differential decreases, the covered orifice is opened to hold mass flow rate nearly constant.

---

*Professor of Aerospace Engineering, University of California at Irvine, Irvine, California. (Consultant at ARTCOR).

In summary, a carefully selected fluidic flow limiter can be a highly reliable device, located between the propellant valve and the evaporator-thrustor assembly, which can greatly improve the transient response of the thrustor as well as the stability of the thrust output during a start-up with water as the propellant.

In addition to the flow limiting devices, a thermal pumping system was studied to determine, for example, whether CO_2 desorbed from molecular sieves could be pumped thermally in a space station application. The thermal pump is considered a possible replacement for mechanical pumps. It involves a cyclic, constant volume cryopumping system which employs space radiators to achieve the cryotemperatures. The frozen CO_2 would be vaporized periodically, using a waste heat loop, to attain sufficient pressure to transfer a large portion of the trapped CO_2 to storage tanks.

Several problems became apparent as the study of this particular thermal pumping system progressed. Small cryopump gas-side volumes and large space radiator areas are required. This requires a long and slender gas-side space which would be susceptible to local blockage by solidified CO_2. Cycle times were found to be long - of the order of three hours. The size and weight of the thermal pump tend to be offset by its capacity for dumping waste heat and thereby supplementing or replacing part of the spacecraft radiator system. Electrical power consumption of mechanical pumps is eliminated by the thermal pump. The thermal pump concept may also prove to be useful for other applications; the large savings in electrical power may make this concept attractive for pumping other gases, as well as CO_2.

INTRODUCTION

Electrical resistance heated rockets, called resistojets, are presently under development for the Space Station/Space Base. These thrustors will utilize the biowaste propellants CO_2, H_2O and CH_4. Considering the integrated EC/LS - resistojet reaction control system operating on these propellants, there are at least two significant problem areas in which thermo-fluidic devices offer performance improvement potential compared to the present baseline system.

The first of these is the problem of mass flow limiting during start-up of the resistojet when the propellant is water. Without adequate mass flow control, water would surge into the evacuated thrustor at start-up. Insufficient energy would be available in the thrustor to supply the large amount of heat of vaporization required for the high liquid mass flow rate with the result that the water propellant would be ejected from the thrustor largely as a liquid. Flow control can be established by using an evaporator stage ahead of the thrustor. One obvious way to prevent the liquid ejection problem would be to preheat the evaporator before commanding propellant flow. With sufficient thermal capacity and preheat, the initial flow surge would be flashed to steam, thereby building up back pressure and effectively controlling the water flow within acceptable limits.

There are, however, several significant disadvantages associated with this obvious solution. Previous experience with evaporator-thrustor assem-

blies has indicated that thrust instabilities occur during the start-up transient caused by traces of liquid water and ice leaving the thrustor. Also, a relatively large evaporator is required, compared to the thrustor heater size; necessitating a relatively long preheat time before the propellant flow can be commanded on.

A fluidic mass flow-limiting device offers the potential advantage of more positive control of the water propellant mass flow rate during the start-up transient, while minimizing the disadvantages associated with the use of an evaporator alone as a flow limiter. One major objective of the present investigation was, therefore, to examine both analytically and experimentally the concept of using one of the various fluidic mass flow limiting devices in conjunction with a biowaste resistojet thrustor operating on water in order to select the optimal configuration for a flow limiter-evaporator-thrustor combination.

A second problem area is the relatively high electrical power consumption of the space station baseline mechanical pumping system required to pump the desorbed CO_2 from the molecular sieve to both intermediate ($\sim$2 atm) and high ($\sim$20 atm) pressure levels for storage, together with the inability of the mechanical pumping system to eliminate the small percentages of O_2 and N_2 which contaminate the desorbed CO_2. The presence of the contaminating gases limits the temperature level and specific impulse potential of metallic biowaste resistojet thrustors because of excessive chemical reactivity at the desired operating temperatures.

A thermo-fluidic cryopumping concept offers the potential for eliminating part or all of the mechanical pumping system, with its high power consumption, while simultaneously providing the means for eliminating the contaminant gases. This concept envisions the use of a space radiator to provide the thermal sink necessary to cryotrap the CO_2 being desorbed from the molecular sieves in the EC/LS system. By periodically valving off the cryotrap and using waste heat from the baseline system Freon-21 loop, the frozen cryotrapped CO_2 could be vaporized, increased in pressure, and pumped to CO_2 storage tanks. A second major objective of the present investigation was, then, to examine the feasibility of this concept in some detail and to compare it with the baseline mechanical pumping system for the desorbed CO_2.

LIST OF SYMBOLS

A	area, m^2
C	specific heat capacity, watt-minute/Kg-°K
C_D	discharge coefficient
D	diameter, m
E	modulus of elasticity, N/m^2
f	ratio or friction factor
F	thrust, N
h	convective heat transfer coefficient, watt/m^2-°K
K	constant
L	latent heat, watt-minute/Kg
m	mass, Kg
$\mathring{m}$	mass flow rate, Kg/sec
M	total mass, Kg
n	sensitivity of $\mathring{m}$ to ΔP
P	pressure, atmospheres or N/m^2 or power, watts
q	heat flux rate, watt/m^2
r	radius, m
R	gas constant
Re_D	Reynolds number based on diameter
t	time, minutes
T	temperature, °K
V	volume, m^3
X	diaphragm deflection, m
α	ratio of sensible to latent heat
ϵ	emissivity
λ	non-condensable mass ratio
μ	Poisson's ratio
ρ	density, Kg/m^3
σ	Stefan-Boltzmann constant, watt/m^2-°K^4
γ	specific heat ratio

Subscripts

C	chamber or control
D	diaphragm
e	effective
fr	flow restrictor
F	Freon 21
m	mass
NC	non-condensable
O	orifice
P	panel
R	relax
S	supply or solid phase
t	thrustor
T	tube or total
v	volume
V	vapor phase

MASS FLOW LIMITING DEVICES

Thrustor Flow Limiting Requirements

Mass flow limiters have been considered in order to provide liquid propellant flow control for resistojet type thrustors. Difficulties were experienced with resistojets operated on water (ref. 1) and hydrazine (ref. 2) using constant pressure type propellant feed systems. Instabilities were observed as the result of the very large starting mass flow rate associated with liquid propellant surging into the empty thrustor. In the case of the H_2O propellant test, the effect was to over-cool the thrustor to the point where liquid water passed through the nozzle throat with the subsequent formation of ice. Flow limiting devices were incorporated into later resistojet designs in order to correct the flow instabilities.

In a concentric-tubes resistojet (ref. 1), the use of a pre-evaporator resulted in good flow limiting, as reported in reference 3. In this case, the pre-evaporator must be hot to insure vaporization of the water before it enters the thrustor. Several minutes are required to preheat the evaporator, while a few watts (2 to 3) will hold it in a ready-to-steam condition for a 10-mlb size thrustor. It should be pointed out that the pre-evaporator concept can be integrated into the thrustor structure and that it has been proven to be an effective flow limiter, but that it also imposes a constraint on the reaction control system by requiring either preheating or sustained heating.

Acceptable flow control with the hydrazine thrustor is reported in reference 4, using a porous element in the propellant inlet region to effect a flow dispersion. This thrustor requires preheating to initiate decomposition of the N_2H_4. The flow limiting in this case is analogous to the pre-evaporator in the water resistojet being necessary to control the decomposition reaction in a stable manner. While a specific liquid flow limiter may be beneficial to the hydrazine resistojet, it does not eliminate the need for preheating. A flow limiter may, however, eliminate the preheating requirement for the water resistojet concept, thereby simplifying the operating mode for this thrustor and greatly improving thrusting response.

Before discussing flow limiter concepts, it is helpful to review briefly the thermal-transient picture of starting a biowaste resistojet. A start-up problem arises when a liquid propellant is to be used because of the necessity to ensure that only vapor is present at the nozzle throat for flow control reasons. This particular problem obviously does not occur with gaseous propellants.

Consider liquid water, for example, being supplied to a cold thrustor by an unrestricted-constant pressure supply. The supply pressure would be the design operating pressure of the thrustor with an allowance for pressure drop in the feed system. When the propellant valve is opened for start-up, the thrustor would fill with liquid water in less than a second and the liquid mass flow rate through the nozzle throat would be of the order of 100 times the design mass flow rate based on high temperature steam flow through the nozzle. In this mode, the thrustor cannot be started. That is, the amount of power required to make steam would be an order of magnitude higher than the design power. If this power were available and were applied, local heat transfer instabilities could result as the transition to steaming occurred and a

heater burn-out would very likely occur. A flow limiting device is required to be able to minimize the starting power requirements and to obtain a stable and safe start-up mode. In addition, a large initial rate of propellant feed is undesirable from a structural point of view. Large inertia forces (water hammering) can occur with unrestricted flow into an evacuated thrustor.

Preheating the thrustor to full operating temperature is not considered practical from power control and thermal shock points of view. Preheating to a nominal ready-to-steam condition of the order of 500°K (900°R) might be feasible. The power required to hold this temperature would be small (a watt or two). A more sophisticated power control system would be required in this case than for full power operation only. However, unless the thrustor incorporates an evaporator section with adequate thermal capacity, an unrestricted propellant feed rate could still thermally swamp the thrustor with liquid flow and again prevent start-up. On the other hand, with a device to limit liquid flow to near the design flow rate, start-up from 500°K, or even a cold start-up, would be feasible and safe.

A resistojet thrustor can be preheated to about 500°K, a ready-to-steam condition, in the order of 10 seconds. A fraction of full design power would be used for preheating to avoid overheating the heater elements. A few watts would then hold the 500°K condition until propellant flow is initiated. The preheated thrustor would make steam instantly when propellant flow is started. Conversely, a cold thrustor with full power and limited propellant flow initiated together would be in a steaming condition in about 5 seconds. Of the order of 100 more seconds would be required to reach design operating conditions. During the 5 seconds of starting from a cold condition, some liquid water could pass through the nozzle throat, and some small ice particles could form downstream of the throat. The ice particles would be expected to break away and not create a problem in the thrustor. However, the passage of liquid and/or ice particles would cause perturbations in thrust which might be undesirable depending on the reaction control system requirements. An advantage of the cold start with flow limiting is control system simplicity. The resulting lower specific impulse with momentary over-thrusting for the first few seconds may be disadvantageous in which case the ready-to-steam preheated start-up with flow limiting would be preferred.

Mass Flow Limiting Concepts

Fixed and variable geometry concepts were considered for flow limiters. Table I lists these concepts, with the fixed geometry devices divided into passive and active categories.

TABLE I
CONCEPTS SUITABLE FOR FLOW LIMITING

1. Fixed Geometry - Passive

   a. Fixed Restrictor
   b. Cavitating Venturi
   c. Non-vented Vortex Amplifier
   d. Vented Fluidic Devices

2. Fixed Geometry - Active

   a. Evaporator
   b. Cavitating Venturi with Vaporization or Ultrasonic Inducer
   c. Electrolysis
   d. Electrokinetic Effect

3. Variable Geometry - Passive and Active

   a. Flow Controller
   b. Positive Displacement Pump
   c. Thermal Expansion Element
   d. Joule Magnetostriction Effect
   e. Wiedeman Effect

The passive devices extract power directly from the flowing fluid, in the form of pressure drop, in order to create the flow limiting effect. The active devices also utilize fluid flow power in addition to other power inputs, typically electrical. Within these classifications, the variable geometry flow controller (3.a.) may be passive (i.e., spring-diaphragm operated valve controlling pressure drop across a restrictor), while the remaining four variable geometry devices are of the active type. The passive concepts listed in table I fall into the class referred to as fluidic devices.* Of the active devices, those with fixed geometries can be considered hybrid-fluidic devices. The variable geometry devices are conventional in the fluid control sense. Those having minor moving parts are also considered hybrid devices. A reasonably constant supply pressure is presumed for all of the devices. A constant pressure supply is not necessary for the flow controller and pump, however.

The purpose of the flow limiter is to minimize flow variations with thrustor pressure. Since the thrustor is downstream of the flow limiter, thrustor pressure is essentially the back pressure on the flow limiter. It ranges from absolute zero before starting to design pressure at final operating conditions. Brief descriptions for the table I concepts are as follows:

1.a. Fixed Restrictor. - This is the simplest of the devices, consisting of a fixed geometry flow resistance such as an orifice, nozzle, or capillary tube.

1.b. Cavitating Venturi. - Physically, this is also a simple device, consisting of a nozzle with a diffuser section (venturi). Functionally, this device is more complex in that it requires cavitation of the flow in the diffuser for flow control.

1.c. Non-vented Vortex Amplifier. - The vortex amplifier is a variable flow restricting device utilizing a constrained vortex. The non-vented vortex amplifier is a mass conservative device in that the usable output mass flow is equal to the total input mass flow.

*Devices without moving parts using moving fluids to perform sensing, control, information processing, and/or actuation functions.

1.d. Vented Fluidic Devices. - These include devices which result in modulated output flow rates as the result of interacting fluid streams. A portion of the throughput is vented, or dumped, and wasted relative to use with a resistojet thrustor. In view of this disadvantage, these devices (proportional, digital, and vented vortex amplifiers) are not considered practical for resistojet flow limiting.

2.a. Evaporator. - This can include the pre-evaporator discussed in the previous section which completely evaporates water being supplied to the thrustor. It can also include a variable degree of partially evaporated water passing through a fixed restrictor to achieve flow limiting. A flow signal feedback would be required on the partial evaporation rate to control flow limiting in the latter case.

2.b. Induced Cavitating Venturi. - This device is essentially the same as item (1.a.) with the addition of some form of excitation to induce cavitation. For the low mass flow rates being considered for biowaste resistojets, it may be difficult to obtain reliable cavitating phenomena in a venturi. Excitation (ultrasonic vibration or local-partial evaporation) may be required to insure repeatable cavitation in a venturi flow nozzle.

2.c. Electrolysis. - Electrolysis of a portion of the water propellant flowing through a restrictor could be used to achieve throttling. This requires water with sufficient conductivity and a flow feedback signal, as in the case of the evaporator (2.a.), to control the rate of electrolysis.

2.d. Electrokinetic Effect. - Water is a polar liquid. In contact with certain solids, some of the liquid molecules become attached to the solid in a preferentially oriented manner. This layer of bound molecules is capable of immobilizing some of the ions existing in the body of the fluid. The total effect is the formation of a double layer of charges. The remaining liquid has a net charge resulting from the abstraction of ions from the liquid body. The liquid can, therefore, be caused to move under the influence of an electric field. Using a capillary bundle or a porous frit, a head of water of the order of one meter can be generated with an electrical potential of the order of 100 volts. While high field strengths would be necessary to generate large pressure differences for adequate resistojet flow limiting, power consumption would be reasonably small.

3.a. Flow Controller. - This device is a conventional fluid dynamic-mechanical device, usually a diaphragm-operated, spring-loaded valve controlling pressure differential across a fixed restrictor. This device is considered as a back-up approach to the fluidic devices.

3.b. Positive Displacement Pump. - A positive displacement pump can provide accurate flow limiting. This concept is given a back-up status in view of the complexity associated with this kind of pumping system.

3.c. Thermal Expansion Element. - Using electrical heating, a bimetallic element can be used to effect flow control through dimensional changes in various flow devices.

3.d. Joule Magnetostriction Effect. - This effect involves a change in physical dimensions of a ferromagnetic material in response to an applied magnetic field. The geometry change in turn can be used as a variable size flow restrictor. Pressure signal feedback would be required to control the applied magnetic field.

3.e. Wiedeman Effect. - The Wiedeman effect is the twist produced in a conductor placed in a longitudinal magnetic field when a current flows through the conductor. Torsional distortion is due to a helical resultant of an impressed longitudinal field on the circular field of the conductor. The material expands or contracts parallel to the helical lines of force producing the twist.

Of these many techniques which might be used to effect flow limiting in a resistojet water propellant feed line, the fluidic mass conservation devices 1.a., 1.b., and 1.c., the hybrid-fluidic devices 2.a. and 2.b., were studies. The so-called hybrid-fluidic controller uses a stiff-highly reliable diaphragm and is comparatively simple relative to more conventional mechanical flow controller devices. Electrolysis was not a candidate because of the low expected conductivity of the water propellant (typically 20 micro-mho per centimeter) and the adverse effect which would occur with the probable variable conductivity. The electrokinetic effect, while a possible solution was also not pursued in view of the high electrical potentials required. The many varieties of variable geometry devices could serve as a source of back-up flow limiting, if required.

By operating with a supply pressure above the thrustor design chamber pressure, and a flow restrictor, reasonable flow control can be accomplished with thrust pressure varying from an initial hard vacuum condition (thrustor off) to the final design pressure (thrustor at steady state conditions). The fixed restrictor is the simplest of the devices being considered and will serve as a baseline concept for performance comparisons.

Mass Flow Limiter Performance

A perfect flow limiter in a hydrodynamic sense would be a device which would hold mass flow rate constant as the pressure differential changed across the device. For a resistojet thrustor operating with liquid water propellant, it is not necessarily desirable to have a perfect flow limiter. The desired flow limiter characteristics depends on the thrustor configuration and on the dynamic requirements of the thrustor. Compared to a given thrustor with propellant controlled by a perfect flow limiter (i.e., constant mass flow rate), the same thrustor with a

less than perfect flow limiter (which would pass an initially higher mass flow rate) could reach steady state operating conditions more rapidly. The actual thrustor response would depend on the electrical power schedule used, the thermal capacity of the thrustor, the flow limiter characteristics, and whether or not preheating is employed before propellant flow is initiated.

The following discussion presents an theoretical examination of the performance to be expected from various candidate flow limiting devices. This is followed by an experimental evaluation of some of the candidates.

Theoretical performance. - Evaporation of liquid water propellant must occur in the resistojet thrustor system in a controlled manner. Either an evaporator must be included in the thrustor heat exchanger assembly as a specific evaporation state, or a separate pre-evaporator must be close-coupled to the resistojet(s), to insure that vaporized water is supplied to the thrustor heat exchanger. An evaporator with sufficient thermal capacity can, in effect, serve as a flow limiter. The thermal capacity, accumulated during pre-heating is necessary to flash the initial surge of liquid water occuring at start up to rapidly build up chamber pressure and thereby restrict any further liquid surges.

A thermal analysis has been conducted to show that a stable start-up can be achieved with a pre-heated evaporator and a constant propellant supply pressure. A typical 25-mlb thrustor condition was considered as follows:

Thrust = 25 mlb
Design Specific Impulse = 250 seconds
Design Mass Flow Rate = .0454 grams per second
Constant Chamber Pressure = 1 atmosphere
Design Chamber Temperature = 1800°K
Design Evaporator Outlet Temperature = 420°K
Inlet Propellant Temperature = 298°K

For these conditions, the steady-state on design power that is put into the propellant by the evaporator is 123 watts and by the final heater stages is 147 watts for a total power input to the propellant of 270 watts. Typical thermal losses at the design condition would be about 30 watts for a total electrical power input of 300 watts.

Figure 1 presents the results of a set of calculations for chamber temperatures varying from a saturated steam temperature (at 1 atmosphere) of 373°K to the design chamber temperature of 1800°K. The power heating the propellant is shown to be relatively constant dropping at first from 271 watts at the saturated steam condition and then increasing to the final design value of 270 watts. The thermal power loss is proportioned with temperature from 5 watts at saturation to 30 watts at the design condition. The mass flow corresponding to a given chamber temperature (an instantaneous value) is shown normalized to the design value. Mass flow is almost 2.3 times the design value for the case of saturated steam leaving the thrustor exhaust nozzle. At the lower temperatures, the specific enthalpy requirement is lower compensating for the higher flow rate and thereby resulting in the relatively constant power heating the propellant. At propellant flow initiation, a flow surge occurs, with a transient mass flow typically 100

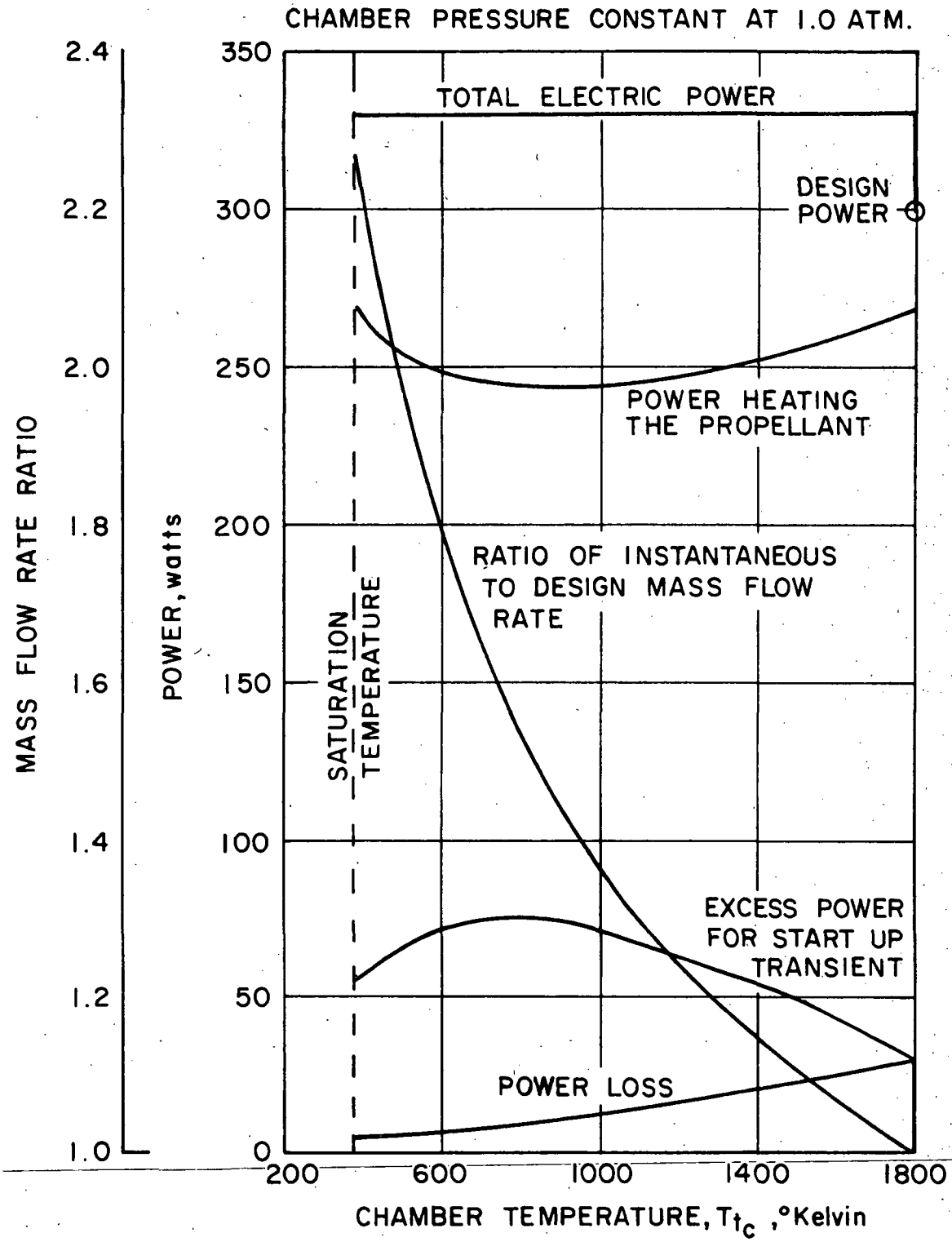

Figure 1.- Mass flow and power characteristics of 25-mlb resistojet starting with water propellant.

times the design mass flow. This very quickly reduces to the 2.3 times value as the initial surge flow is flashed to steam. For simplicity, this transient is not indicated in the figure 1 representation, and chamber pressure is assumed constant at a typical value of 1.0 atmospheres.

A rigorous transient analysis has not been made; however, a close approximation of the time to reach design conditions can be made from figure 1. Consider, for example, a resistojet which includes an integral pre-evaporator. Prior to commanding propellant flow to the thrustor, the evaporator would be preheated to about 420°K. Some preheating of the final heater stages would also occur. Consider that the thrustor power for the final heater stages is commanded on with propellant flow initiation. Chamber temperature would typically begin at or slightly above the saturation temperature. Assume that a total electric power input of 330 watts (30 watts above design) is used for the heat up transient. The excess power available for heating the thrustor structure and increasing the chamber temperature would be the difference between the total electric power input and the sum of the power heating the propellant and that which is lost:

$$P_{excess} = P_{electric} - \left[P_{heating\ propellant} + P_{loss}\right] \qquad (1)$$

The excess power is shown in figure 1 and is adequate to effect a rapid start-up transient to the design condition. A stable start up is assured by the always positive value of the excess power. On an average, for the case considered, about 60 watts of excess power are available. A typical 25 mlb thrustor would require about 6000 watt-seconds of additional thermal inventory to power-up from the start to design conditions. The time to effect the start-up would then be 6000/60 to 100 seconds. Upon reaching the design condition, total power would be reset to the design value of 300 watts as indicated in figure 1. A shorter start-up transient would occur with a higher power input and/or a thrustor with a smaller thermal capacity.

The above discussion is presented to indicate that pre-evaporators can be used effectively to achieve a stable start-up with water propellant supplied at constant pressure. The evaporator must, of course, be preheated to a ready-to-make-steam condition prior to initiating propellant flow. The preheating would normally require from 100 to 200 seconds depending on the evaporator design. For a typical thrustor, final design conditions are reached after about 100 seconds additional time. During this start up interval specific impulse would increase from about 120 seconds (near-saturated steam conditions) to over 250 seconds at design conditions. The effective specific impulse during the start-up transient would be less than 200 seconds, which may not be significant in terms of long thrusting times contemplated for the space station biowaste resistojets.

A more effective flow limiting device, while not absolutely necessary, can improve the propellant-thrustor system performance in the following ways:

1. The start-up transient of the biowaste resistojet with water propellant can be shortened by limiting the initial high propellant surge flow thus not requiring as high a thermal capacity in the evaporator stage.

2. In keeping with item (1), a smaller-lighter mass evaporator stage can be used.

3. A higher degree of reliability would be offered with the flow limiter in the event adverse start up conditions occurred (i.e. inadequate evaporator stage warm up).

4. The sensitivity of thrust to changes in supply pressure can be reduced by introducing a flow limiting device.

The first three items are obvious from the discussion above. Item 4 is shown to be true in the discussion which follows.

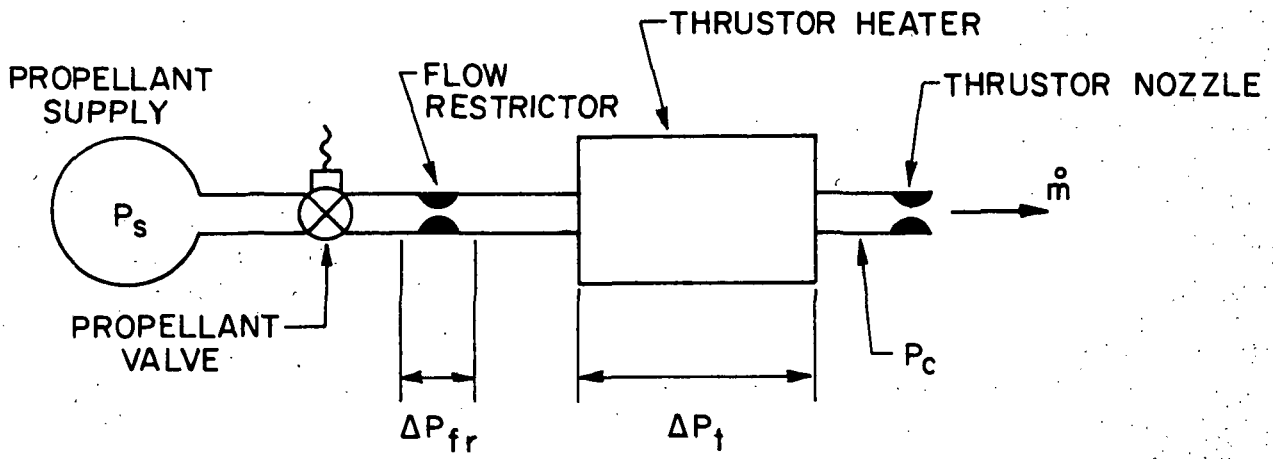

Figure 2.- Flow restrictor-thrustor pressure drop model.

Figure 2 indicates schematically the relative placement of a flow restrictor in relation to the propellant supply and thrustor. The pressure losses across the flow restrictor ΔP_{fr} and the thrustor ΔP_t which result from a mass flow rate $\dot{m}$ are indicated. The supply pressure necessary to achieve a chamber pressure of P_c is given by:

$$P_s = P_c + \Delta P_{fr} + \Delta P_t \qquad (2)$$

The thrustor pressure drop is essentially a laminar conduit type loss for which ΔP_t is proportional to mass flow rate.

$$\Delta P_t = K_1 \dot{m} \qquad (3)$$

For a contraction-expansion type flow restrictor, for example,

$$\Delta P_{fr} = K_2 \dot{m}^2 \qquad (4)$$

Thrust F of the resistojet is proportional to mass flow rate for specific impulse assumed constant. The assumption of specific impulse constant follows an assumed constant chamber temperature resulting from controlling electric power to hold a constant final stage heater temperature. Since mass flow leaving the thrustor exhaust nozzle for constant geometry and constant temperature is proportional to chamber pressure, then

$$F = K_3 \dot{m} \tag{5a}$$

$$= K_4 P_c \tag{5b}$$

Substituting equation (2) into equation (5b), thrust relates to the supply pressure and pressure losses as follows:

$$F = K_4 \left(P_s - P_{fr} - \Delta P_t\right) \tag{6}$$

Differentiating equation (6) and dividing by equation (6) to obtain a sensitivity expression for thrust

$$\frac{dF}{F} = \frac{K_4}{F} dP_s - \frac{K_4}{F} d(\Delta P_{fr}) - \frac{K_4}{F} d(\Delta P_t) \tag{7}$$

Relating the pressure loss differentials to thrust from equations (3), (4) and (5a), solving for the sensitivity of thrust to a change in supply pressure, and simplifying, the following is found

$$\frac{dF/F}{dP_s/P_s} = \frac{P_s}{P_c + \Delta P_t + 2\Delta P_{fr}} \tag{8}$$

which reduces further to:

$$\frac{dF/F}{dP_s/P_s} = \frac{1}{1 + \Delta P_{fr}/P_s} \tag{9}$$

A plot of equation (9) is presented in figure 3. It shows that the percentage change in thrust due to a percentage change in supply pressure is attenuated by the pressure loss across a flow restrictor. Note that the pressure loss in the thrustor does not affect the sensitivity of thrust to supply pressure. This is a consequence of the laminar conduit type pressure loss assumed (equation 3) which is realistic for the 25-mlb size thrustor. The figure 3 curve is for a contration-expansion type flow restrictor such as a nozzle or orifice. Obviously the limiting value of $\Delta P_{fr}/P_s$ of 1.0 in figure 3 is unrealistic, since it corresponds to zero pressure drop in the

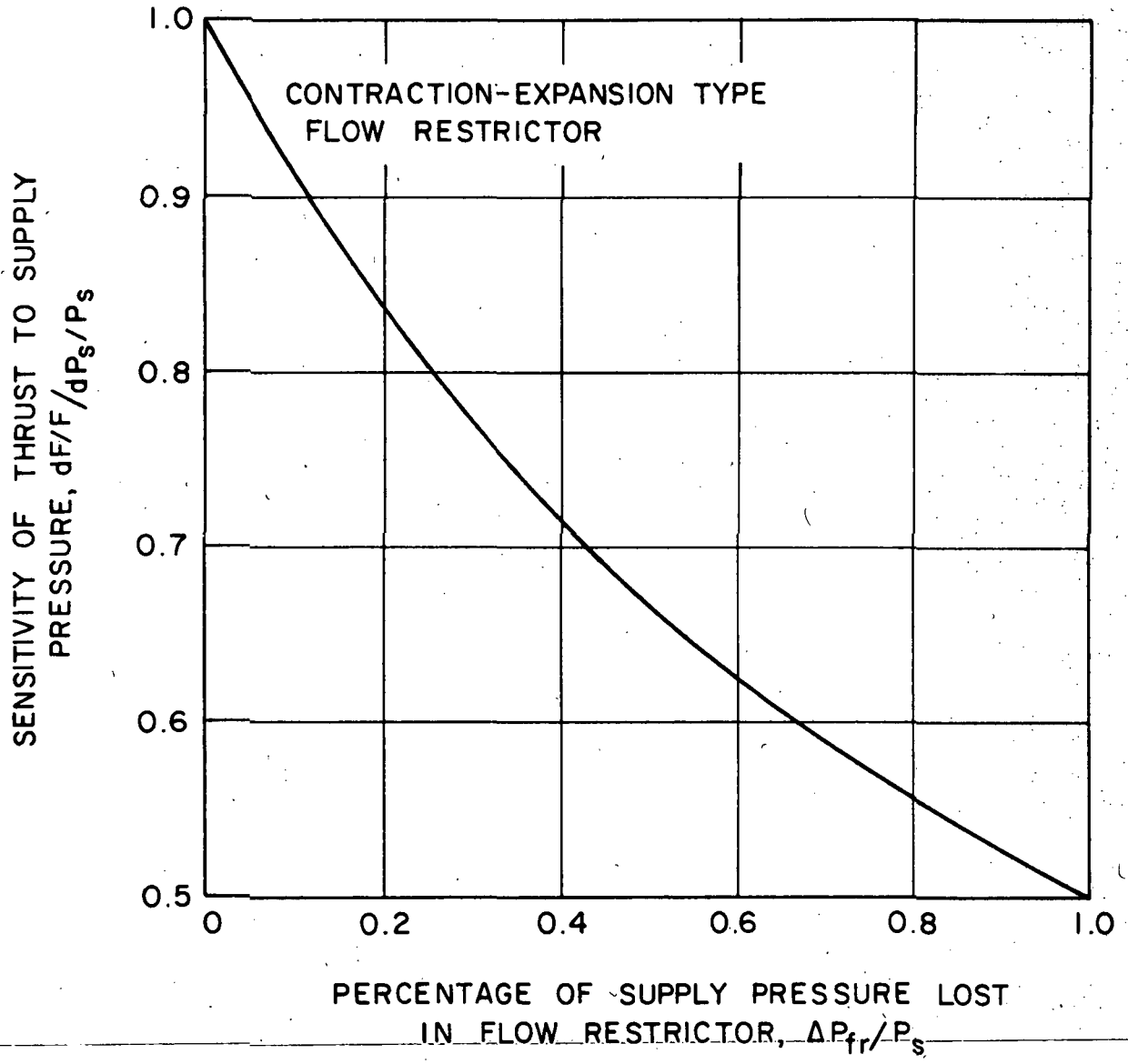

Figure 3.- Effect of supply pressure changes on thrust for various flow restrictor pressure losses.

thrustor. Reasonable values of $\Delta P_{fr}/P_s$ are in the range of 0.4 to 0.5, for which the effect of supply pressure on thrust is attenuated about 30%. This means that for a given allowable thrust error due to chamber pressure variations, the supply pressure allowable tolerance limits can be broadened by about 30% with the use of a flow restrictor.

The pressure differential across a fixed restrictor varies with mass flow rate. The relationship between pressure differential and mass flow rate depends on both the type of restrictor and the type of flow (i.e., whether it is laminar or turbulent). Fixed restrictors can be geometrically classified as: (1) laminar conduit, (2) turbulent conduit, and (3) contraction-expansion devices.

Laminar conduit includes capillary tubes and porous elements in which laminar flow persists and mass flow rate is linearly proportional to pressure differential.

$$\dot{m} \sim \Delta P \qquad \text{(laminar conduit)} \tag{10}$$

Equation (10) follows from the Darcy Equation for which

$$\Delta P \sim f\dot{m}^2 \tag{11}$$

and the friction factor f for laminar flow in conduit is

$$f = \frac{64}{Re_D} \sim \frac{1}{\dot{m}} \tag{12}$$

For smooth conduit with turbulent flow at Reynolds numbers below 10^5, the friction factor is typically given by the Blasius relation

$$f \sim R_{ed}^{-1/4} \sim \dot{m}^{-1/4} \tag{13}$$

In this case

$$\dot{m} \sim \Delta P^{4/7} \qquad \text{(turbulent conduit)} \tag{14}$$

For a contraction-expansion device, such as a nozzle or an orifice, with negligible viscous loss,

$$\dot{m} \sim \Delta P^{1/2} \qquad \text{(contraction-expansion)} \tag{15}$$

which follows from the flow equation for such a device

$$\dot{m} = C_D A \sqrt{2\rho\Delta P} \tag{16}$$

Mass flow rate of all of these flow limiting devices is a function of the pressure differential across the device and can be generalized by the equation

$$\dot{m} = k(\Delta P)^n \tag{17}$$

The exponent n is just the sensitivity of the mass flow rate $\dot{m}$ to the pressure differential ΔP, that is

$$n = \frac{d\dot{m}/\dot{m}}{d\Delta P/\Delta P} \tag{18}$$

The sensitivities for the three flow limiting devices described above are as follows:

Device	Sensitivity, n
Laminar Conduit	1.00
Turbulent Conduit	0.57
Contraction-Expansion	0.50
Perfect Flow Limiter	0.00

The sensitivity of zero for the so called "perfect" flow limiter is shown for comparison. In the perfect device, mass flow rate is uneffected by changes in pressure differential. Of the real fixed restrictors, the contraction-expansion device offers the lowest sensitivity and provides the best flow limiting. Figure 4 shows that for a given flow restrictor pressure recovery P_2/P_1, the initial to final mass flow rate ratio is lowest for the contraction-expansion device and highest (worst) for the laminar conduit device. A turbulent conduit condition is not likely to occur for the flow conditions typical of a 25-mlb biowaste resistojet. The initial to final mass flow ratio is the starting mass flow rate entering an evacuated thrustor ratioed to the final operating condition mass flow rate.

Fixed restrictor sizes would be small for biowaste resistojets. For the mass flow ratio of 2.0, and a thrustor pressure of P_2 of 2 atmospheres, for example, the following are typical throat sizes:

Thruster Size, mlb	Throat Diameters, cm (inches)	
	Orifice	Nozzle
10	.0055(.0022)	.0047 (.0019)
25	.0088(.0035)	.0075 (.0029)
50	.012 (.0049)	.011 (.0041)
100	.018 (.0069)	.015 (.0059)

Below the 25 mlb thrustor size, the flow restrictor becomes undesirably small. As the mass flow ratio allowed increases, pressure recovery improves and restrictor sizes increase relative to the above values. Filtration upstream of the restrictor becomes essential with these small size throat diameters.

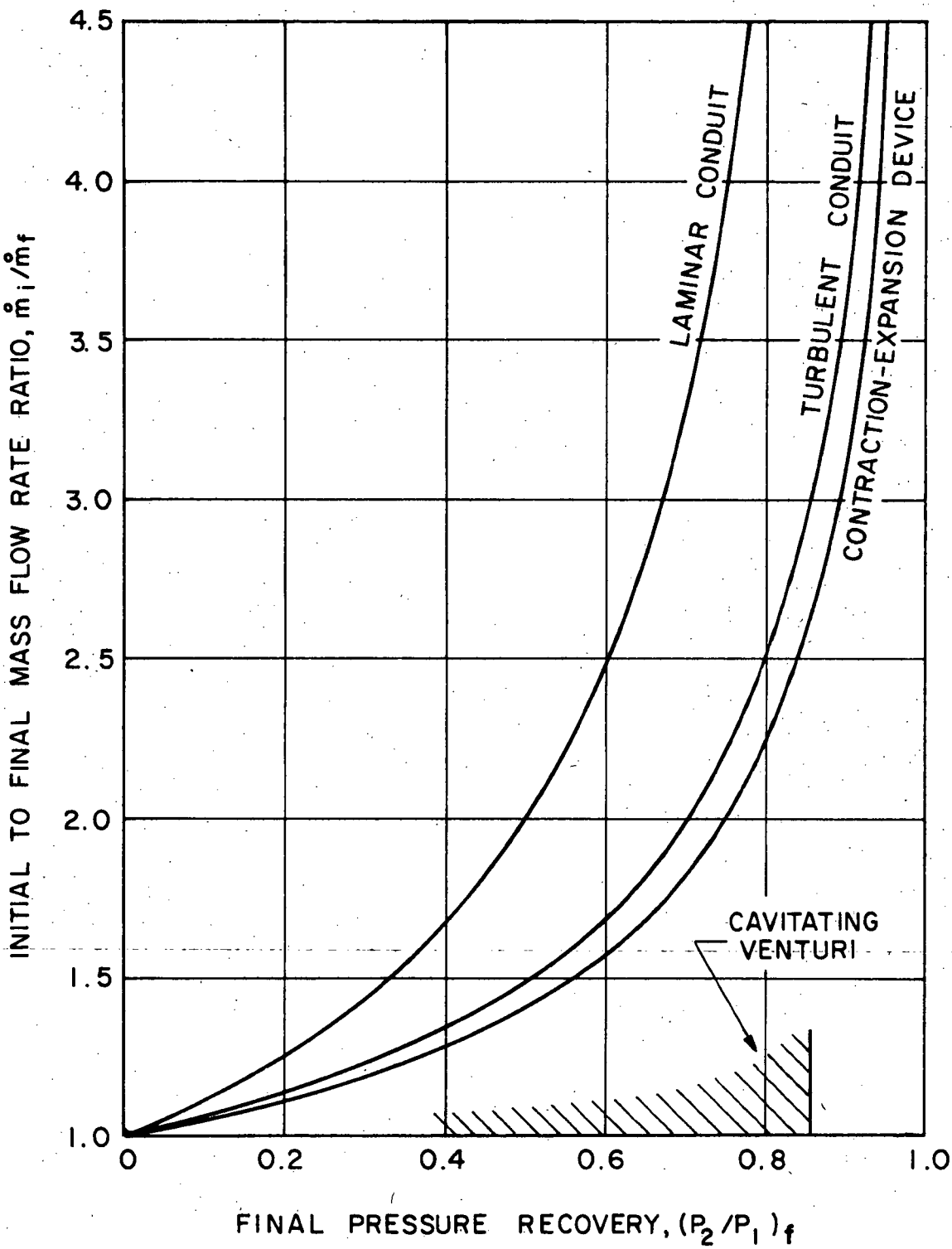

Figure 4.- Flow characteristics of simple flow restrictors.

The venturi, a flow nozzle followed by a diffuser, offers excellent flow control at high pressure recovery when used with cavitating liquid flow. Typical of current cavitating venturi technology is a mass flow ratio approaching unity with a pressure recovery as high as 0.85 as reflected in figure 4. The following equation describes the pressure variation occurring at the nozzle inlet (station 1), the nozzle throat (station 2), and the diffuser exit (station 3) of a venturi:

$$P_1 = P_2 + \frac{\rho u_2^2}{2} = P_3 + \Delta P_{2-3} \qquad (19)$$

Equation (19) is the Bernoulli equation with the following assumptions:

a. Negligible velocities at stations 1 and 3.
b. Negligible viscous loss from station 1 to 2.
c. Negligible mass flow of vaporized fluid at stations 1, 2, and 3.

In equation (19), P represents the local static pressures (equal to the local stagnation pressures at stations 1 and 3), ρ is the liquid density, and u is the velocity.

ΔP_{2-3} represents the pressure loss in the diffuser. It is this term which varies with different degress of cavitation to adjust to variations in P_3. While in a cavitating mode with constant inlet pressure P_1, the sum of P_3 and ΔP_{2-3} remains constant over a considerable range of P_3. Typically, the pressure recovery P_3/P_1 ranges from 0.85 to about 0.10 for constant mass flow rate at constant inlet pressure as cavitation increases. During cavitation, P_2 is equal to the vapor pressure of the liquid and remains constant, as does u_2, for constant inlet pressure. During the initial start-up of a thrustor using a cavitating venturi for flow limiting, hysteresis and cavitation delay may occur which can result in an initially higher mass flow rate. This delay phenomenon is more likely to occur with smaller size cavitating venturis.

Cavitating venturis have been used in throat sizes ranging down to about 0.3 centimeter (0.12 inches). For the biowaste resistojet, venturis smaller by as much as two orders of magnitude may be required. In this situation, scaling effects, including viscous effects and time delay effects, become critical, and it is not clear whether a miniature venturi will cavitate reliably; nor is the resulting initial to final mass flow ratio predictable.

Cavitation conditions are best expressed by the cavitation parameter

$$K = \frac{P_1 - P_v}{\frac{\rho u_2^2}{2}} \qquad (20)$$

where P_v is the vapor pressure of the liquid. Equation (20 follows from the left hand side of equation (19) with P_2 equal to P_v. Ideally, cavitation would

occur when K drops to or below unity. Usually, cavitation effects present problems which investigators try to avoid, and hence, experimental data reflect a trend toward making K as low as possible. Data on cavitation near submerged objects reflect a definite trend toward lower K for smaller sizes. In the case of a deliberate cavitating venturi for flow limiting purposes, as high a K as possible is preferred to keep the venturi a reasonable size (not too small).

No adequate scaling criteria are available for predicting cavitation performance for flow limiter mass flow rates of interest. Some indication of the effect of size may be obtained from work on submerged bodies. In terms of a predicted value of the cavitation parameter K_p based on a pressure distribution about the body, the incipient cavitation parameter K_i suggested in reference 5 is given by

$$K_i = K_p - \frac{\text{Constant}}{(u_0 d)^{1/2}} \tag{21}$$

where d is the diameter of the body, and u_0 is a reference velocity. Reference 6 suggests a similar relationship for turbulent flow, and the first power on $u_0 d$ for laminar flow. These would suggest that K_i decreases as size decreases.

In general, the following factors relative to a flow limiter design affect cavitation:

a. Nuclei are necessary for cavitation. These may include gas in the liquid and those nuclei fixed on solid surfaces.

b. Viscosity and surface tension are important in the initial growth rate of vapor bubbles and decrease their rate of growth.

c. Turbulence (and roughness which induces turbulence) enhances the inception of cavitation.

d. Inception of growth of nuclei depends very little on the duration of a favorable (suitably low) pressure. Subsequent growth, necessary for effective flow control in a cavitating venturi, does depend on the duration of a favorable pressure, however.

e. Hysteresis occurs in cavitation, is a scale effect becoming greater for decreased geometric size, and depends on the circulating and surface-bound nuclei.

Data obtained by Kermeen, et al., (ref. 7), and given in reference 8, indicate how cavitation numbers for a particular submerged body decrease from about 0.65 for a 2-inch diameter body to about 0.4 for a 0.25-inch diameter body. For a biowaste resistojet limiter of the cavitating venturi type, an order of magnitude guesstimate of 0.1 is made for the cavitation parameter to get an idea of the size of the venturi throat. Using the continuity equation

$$\dot{m} = \rho u_2 C_D A_2 \tag{22}$$

and the cavitation parameter, equation (20), the following expression for effective diameter is derived:

$$D_{eff} = \left(\frac{4\mathring{m}}{\pi}\right)^{1/2} \left[\frac{K}{2\rho(P_1 - P_v)}\right]^{1/4} \tag{23}$$

$C_D A_2$ is the effective area; therefore, the geometric diameter is given by:

$$D_{geom} = \frac{D_{eff}}{\sqrt{C_D}} \tag{24}$$

Figure 5 presents the effective throat diameter for a cavitating venturi with the assemed K value of 0.1 for cold water (25°C). Supply pressure P_1 is a parameter. Mass flow rates for 10 and 50-mlb size thrustors, based on a specific impulse of 250 seconds, are indicated as well as some typical Reynolds numbers based on throat diameter. For example, a venturi for a 50-mlb thrustor with a supply pressure P_1 of 2.0 atmospheres would have a throat diameter of the order of 0.0043 cm (0.0017 inches) with a Reynolds number in the transition regime. Therefore, the cavitating venturi, like the fixed resistor, may have an undesirably small throat size. Compared to the orifice and nozzle fixed restrictions, venturis are smaller by virtue of the higher throat velocities, yet they incur smaller pressure losses as a result of good pressure recovery.

Sensitivity of a cavitating venturi to changes in vapor pressure P_v can be shown to be small. From the mass flow equation for laminar flow through the venturi nozzle throat, for example,

$$\mathring{m} = k(P_1 - P_v) \tag{25}$$

where the density, throat area, discharge coefficient, and cavitation parameter are taken as constants. Actually, second order effects can occur with ρ, C_D, and K. Sensitivities of mass flow rate with supply pressure P_1 and vapor pressure P_v are as follows:

$$\left[\frac{d\mathring{m}/\mathring{m}}{dP_1/P_1}\right]_{P_v} = \frac{P_1}{P_1 - P_v} \tag{26}$$

$$\left[\frac{d\mathring{m}/\mathring{m}}{dP_v/P_v}\right]_{P_1} = \frac{-P_v}{P_1 - P_v} \tag{27}$$

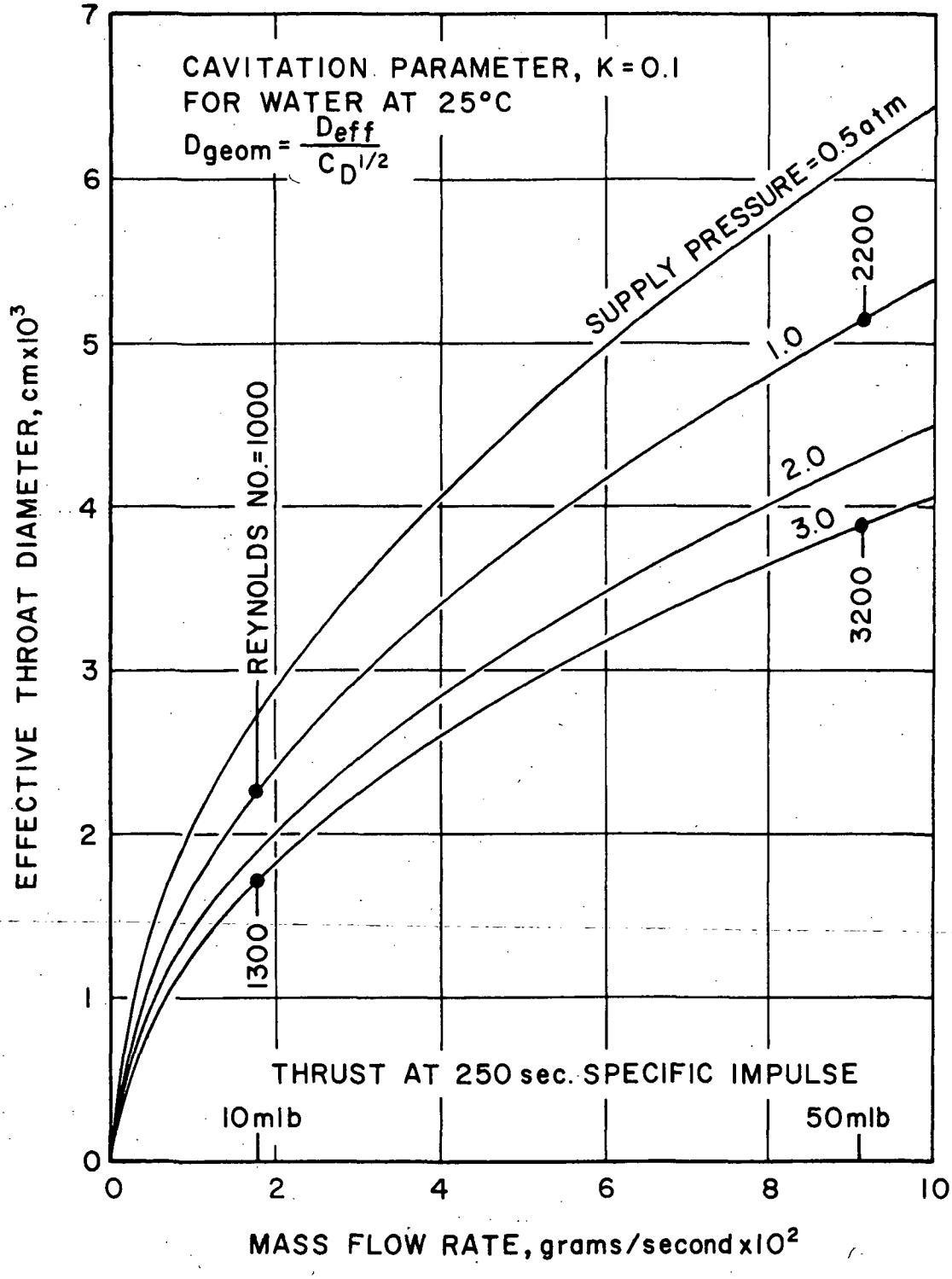

Figure 5.- Estimated cavitating venturi size.

For typical conditions (25°C water and 2 to 3 atmosphere supply pressure), sensitivity to supply pressure is about 1.0 while sensitivity to vapor pressure is low at about -0.01. For turbulent flow, sensitivities can be shown to be about one-half those for laminar flow. These sensitivity values show that supply pressure must be maintained relatively constant for good flow limiting and control. On the other hand, changes in vapor pressure due to temperature changes are not a critical factor. For a ±25°C change in temperature, mass flow rate changes less than ±2.5 percent for laminar flow. The cavitation parameter will undoubtedly be a variable in the small venturi size and may present a problem which can only be evaluated from experimental data.

Thus far, the discussion on cavitating venturis has been limited to passive devices. In the small sizes required for biowaste thrustors, it may be necessary to use active devices in which some form of excitation is used to induce cavitation. This offers the advantage of removing or minimizing hysteresis effects and time delay effects. Cavitation can be induced by acoustic (including ultrasonic) energy, and also possibly by partial evaporation of the fluid stream in the vicinity of the venturi throat. Exploratory type tests using ultrasonic excitation to induce cavitation in small orifices and nozzles are discussed in the next section.

Another technique which was considered to enhance cavitation in a small venturi involves superimposing a swirl or a vortex-like flow on the axial venturi flow. The swirl is used to increase the local velocity for cavitation while decreasing the axial velocity associated with throughput. In this way, the geometric diameter of the venturi could be increased. Swirl could have an adverse effect on the diffuser pressure recovery, however, which is of primary importance in proper flow limiting with a cavitating venturi.

Swirl could be obtained by injecting the liquid supply tangentially into a vortex chamber forming the entrance plenum to the venturi throat. For the small flow of interest, viscous effects will be predominant and free vortex flow would not occur. Viscous coupling causes the flow to revert toward a forced vortex condition with lower swirl velocities near the region of interest - the venturi throat. Vector diagram considerations indicate that even with a substantial swirl component of velocity, the diameter of the venturi throat cannot be increased by more than a factor of 2. With a diameter increase of a factor of 2, the swirl velocity is theoretically above 95 percent of the cavitation velocity. Inadequate margin exists in this case and cavitation could begin upstream of the venturi throat-diffuser section, causing adverse flow limiting performance.

While swirl in a cavitating venturi does not appear to aid significantly the critical size situation for the 10 to 50-mlb class of thrustors, it may be useful in a vortex amplifier. Flow throttling and control can be obtained by varying the amount of swirl imposed on radial flow throughput in a vortex amplifier. This device has been considered as an alternate flow limiting device which does not generally use cavitation for flow control. In this device, the swirl is not used to affect a higher throat velocity for purposes of cavitation enhancement; rather, the swirl, through centripetal forces, imposes a back pressure on the fluid supply to affect flow throttling. Cavitation coupled with a standard vortex amplifier (non-vented type) may have additional advantages.

The pre-evaporator, close-coupled or integrated into the thrustor, is a unique flow limiter. Initial mass flows would be relatively quite high as the pre-evaporator fluid inventory is established. Initial vapor passing to the thrustor may partially condense, resulting in increased flow rates relative to a non-condensing situation. However, the vapor carries thermal energy into the thrustor for a more rapid heat-up. Also, at design conditions, pressure recovery can approach 100 percent (low loss) with a properly designed pre-evaporator. As a result of initial condensation in the thrustor, some water flow-icing phenomena can occur in the thrustor nozzle. This is not dangerous to the thrustor, but does result in erratic thrust levels at start-up. Erratic thrust levels (momentary bursts to higher than design thrust) would also occur with a cold thrustor started up with a good mass flow limiter.

A pre-evaporator tested under various flow and power conditions with a 10-mlb biowaste resistojet is discussed in reference 9. This pre-evaporator was found to be unstable with gas-liquid mixtures in that a piston effect occurred in which water slugs were pushed forward by the gas causing pressure surges. The evaporator did function properly with either gas or water separately. The flow instabilities observed (ref. 9) could result in an adverse thermal transient resulting in a thrustor-heater over temperature or burn-out situation. Conceivably, a two-phase condition could occur during propellant change-over, for example, or it may be desirable for some applications to handle two-phase flows. In effect, these instabilities, if allowed, would require a derating of the thrustor to provide sufficient tolerance against burn-out.

It appears that an evaporator should not be the sole flow limiting device used. Instead, one of the other types of flow limiting devices previously described should be employed, preferably in conjunction with an evaporator. A pre-evaporator section integrated with the thrustor heater is advantageous. Thermal leakage into the heater could preheat the entire thrustor to a ready-to-steam condition. However, this requires anticipating the thrusting command or holding the preheated condition indefinitely. The mass flow limiter provides two advantages. First, the thrustor can be reliably commanded on from a cold condition; and secondly, it improves the reliability of a pre-evaporator type thrustor by serving as a backup flow control in the event the evaporator is not sufficiently heated.

A hybrid flow limiter was designed in order to achieve improved flow limiting performance over that of a contraction-expansion device (the best of the fixed geometry devices). The hybrid device was considered in order to take advantage of the performance characteristics of a moving element while remaining simple and highly reliable. Compared to an orifice, for example, the hybrid was conceived to significantly improve flow limiting performance without introducing a significant reduction in restrictor size and thereby incurring a blockage due to particle contamination penalty.

A device utilizing a stiff, low-stressed metal diaphragm was conceived and is depicted in the figure 6 schematic. The key elements of the hybrid flow limiter are the flexing diaphragm containing one off-center orifice, an orifice plate containing two orifices (one centered and one off-center), and a spacer ring to space the diaphragm off of the orifice plate. The orifice plate is backed up by a thicker plate to prevent flexing of the orifice plate under pressure loading.

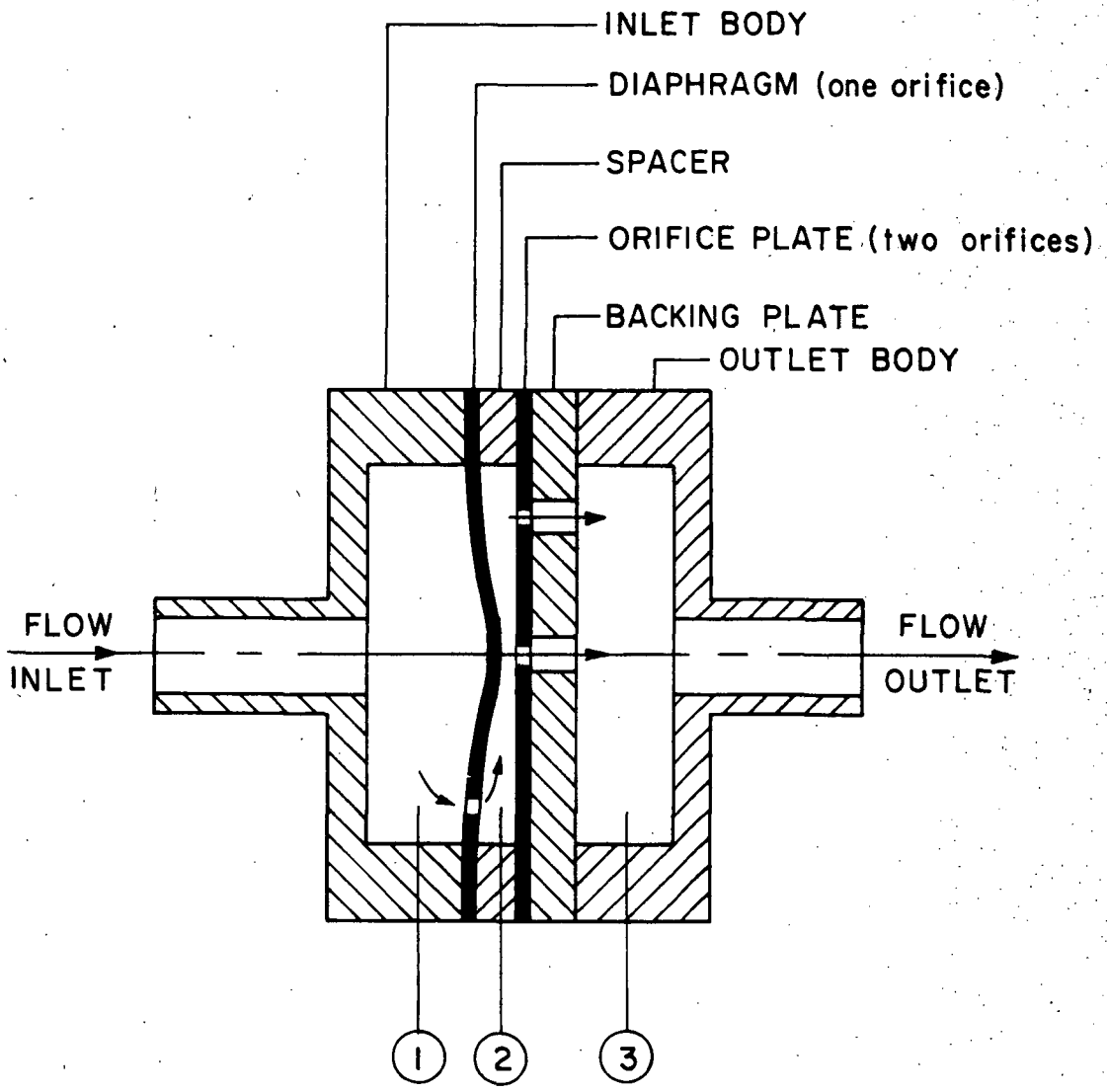

Figure 6.- Hybrid flow limiter schematic.

The hybrid flow limiter would be located in the flow restrictor position shown in figure 2. Prior to turning on the thrustor, the limiter would be evacuated to the space vacuum through the thrustor. Upon commanding water propellant flow, an initial maximum pressure differential $(P_1 - P_2)_i$ would occur across the diaphragm causing it to flex in the downstream direction and throttle the center orifice in the orifice plate. The flow rate would be defined by the resistance of the two off-center orifices flowing in series, with a small or zero contribution from the center orifice which is also in series with the diaphragm orifice. As thrustor chamber pressure (essentially P_3) increased, flow rate would be reduced, as with a fixed contraction-expansion device. However, the flow reduction would be accompanied by a reduction in $(P_1 - P_2)$, causing the diaphragm to relax, uncovering the center orifice and, in effect, causing mass flow rate to increase relative to a fixed restrictor. Over the pressure operating range of the flow limiter, a flatter, less sensitive flow curve would result.

The hybrid flow limiter performance can be predicted analytically using flow equations for the orifices and the deflection formula for the diaphgragm. The simplified derivation which follows will assume that the off-center orifices are not restricted as the result of diaphragm flexing. This would be the case if the off-center orifices were located at the far edges of the diaphragm and orifice plate, or if these orifices were recessed with appropriate counter bores.

Assuming that the diaphragm deflection and mass flow rate will make a smooth transition from an initial to a final pressure differential condition, it is only necessary to evaluate the flow equations at these limiting conditions to establish the working forces on the diaphragm. Let the orifice plate holes be identical in size with the flow area A_O. Let A_D represent the diaphragm hole flow area. Further assume that the diaphragm will close off the center orifice at the initial flow condition. The following equations define the initial and final mass flow conditions:

$$\mathring{m}_i = KA_D \, (P_1 - P_2)_i^{1/2} = KA_O \, (P_2 - P_3)_i^{1/2} \tag{28}$$

$$\mathring{m}_f = KA_D \, (P_1 - P_2)_f^{1/2} = 2KA_O \, (P_2 - P_3)_f^{1/2} \tag{29}$$

In the final flow condition reflected by equation (29), it is assumed that the diaphragm completely uncovers the center orifice. The constant K is taken to be the same for equations (28) and (29) and includes a square root of density term and a flow discharge coefficient term. In effect then, the discharge coefficient is assumed to be the same for each of the orifices in both limiting modes. For incompressible flow and similarly sized orifices, this is a reasonably good assumption.

Solving equations (28) and (29) for the respective mass flow rates in terms of the overall pressure differential $(P_1 - P_3)$

$$\mathring{m}_i = KA_D \left[\frac{(P_1 - P_3)_i}{1 + \left(\frac{A_D}{A_O}\right)^2} \right]^{1/2} \tag{30}$$

$$\mathring{m}_f = KA_D \left[\frac{(P_1 - P_3)_f}{1 + \left(\frac{A_D}{2A_O}\right)^2} \right]^{1/2} \tag{31}$$

The initial to final mass ratio becomes

$$\frac{\mathring{m}_i}{\mathring{m}_f} = \left[\frac{1 + \left(\frac{A_D}{2A_O}\right)^2}{1 + \left(\frac{A_D}{A_O}\right)^2} \right]^{1/2} \left[\frac{1}{1 - \frac{P_{3_f}}{P_1}} \right]^{1/2} \tag{32}$$

where P_{3_i} has been taken as zero (thrustor evacuated initially).

The working pressure differentials across the diaphragm are

$$(P_1 - P_2)_i = \frac{P_1}{1 + \left(\frac{A_D}{A_O}\right)^2} \tag{33}$$

$$(P_1 - P_2)_f = \frac{(P_1 - P_3)_f}{1 + \left(\frac{A_D}{2A_O}\right)^2} \tag{34}$$

The supply pressure P_1 is a constant for the thrustor application. Relating equation (31) for the final flow condition to an equivalent effective orifice area A_e for which the mass flow rate is given as

$$\mathring{m}_f = KA_e (P_1 - P_3)_f \tag{35}$$

the effective orifice diameter is found to be

$$D_e = \frac{D_D}{\left[1 + \frac{1}{4}\left(\frac{D_D}{D_O}\right)^4\right]^{1/4}} \tag{36}$$

Typically, the diaphragm orifice diameter D_D is 33% larger than the orifice plate hole size D_O, and D_e is found to be 87% of D_D, or 15% larger than D_O. Therefore, the minimum orifice size D_O is close (within 85%) to the effective orifice diameter D_e of the device, and a flow blockage problem is not incurred. The closing down of the orifice plate center hole occurs only during the start-up transient. During steady-state, both orifice plate holes are open. Therefore, the center orifice is not considered susceptible to blockage relative to the effective diameter of the device.

The diaphragm deflection due to pressure differential loading is represented by equation (6) of Chapter 10 in Roark (ref. 10) for a circular plate, uniformly loaded, and with clamped edges. Solving Roark's equation for the diaphragm radius r

$$r = \left\{\frac{16E}{3(P_1 - P_2)(1 - \mu^2)}\left[\frac{x}{t} + 0.488\left(\frac{x}{t}\right)^3\right]\right\}^{1/4} t \tag{37}$$

Laminar flow will occur in a hybrid flow limiter sized for the biowaste resisto-jet. The center hole in the orifice plate can be considered to be fully open when the diaphragm stands off a distance x_R for which the gap peripheral area A_P is equal to the hole area A_O.

$$A_P = \pi D_O x_R$$

$$A_O = \frac{\pi}{4} D_O^2$$

For $A_P = A_O$, then

$$x_R = D_O/4 \tag{38}$$

Considering that the diaphragm has a total deflection of x_T initially and just closes the center orifice, then it is required to relax through the x_R distance for the final flow condition. For deflections small compared to the diaphragm thickness t, equation (37) indicates a direct proportionality between deflection x and load $(P_1 - P_2)$. Therefore, the total required diaphragm deflection x_T can be estimated to be

$$x_T = x_R \frac{(P_1 - P_2)_i}{(P_1 - P_2)_i - (P_1 - P_2)_f} \tag{39}$$

For typical hybrid flow limiter conditions corresponding to prototype hardware tests discussed in the next section, solutions to equations (32), (33), (33) minus (34), (36), (37) and (39) are shown graphically in figure 7. The required diaphragm radius r follows from equation (37) using the total deflection x_T from equation (39) and the initial pressure differential $(P_1 - P_2)_i$ which causes the total deflection. As thrustor chamber pressure builds up, the diaphragm relaxes an amount x_R when the final pressure differential of $(P_1 - P_2)_f$ is reached.

The variables listed in figure 7 include a modulus of elasticity and Poisson's ratio for corrosion resistant steel, a supply pressure of 3.06 atmospheres (45 psia) and a final thrustor chamber pressure of 2.04 atmospheres (30 psia). An orifice plate hole size D_0 of 0.0152 cm (0.006 inches) was chosen as convenient for fabrication of the prototype unit. The relaxation distance x_R follows from equation (38). A diaphragm thickness t of 0.0254 cm (0.010 inches) was chosen to result in a reasonable prototype size. The prototype unit was fabricated with a diaphragm orifice size of 0.020 cm (0.0079 inches). According to figure 7, a total deflection of 0.0154 cm is required and the $(x/t)^3$ term in equation (37) is about 1/3 of the first order term. Thus, equation (39) provides an estimate of x_T. A more accurate analytical evaluation of the x_T required can be obtained by carrying both terms in equation (37) when deriving an expression for x_T in terms of x_R and the pressure load terms. The equation (39) simplification is suitable for sizing prototype hardware where the final adjustments are made by selecting a spacer of appropriate thickness.

The stress in the deflected diaphragm due to pressure loading can be evaluated using the equations of reference 10. For the prototype hybrid flow limiter, under worst case conditions, the total stress in the diaphragm was found to be about 1.1×10^8 N/m^2 (16,000 psi). This is well below the endurance limit for corrosion resistant steel. Cyclic lifetimes measured in millions of cycles should be possible, indicating that the hybrid flow limiter should be a highly reliable device.

Note from figure 7 that a mass flow ratio (initial to final) of the order of 1.2 is possible with the hybrid flow limiter. For the figure 7 conditions (final pressure recovery of 67%), a contraction-expansion device would result in a mass flow rate ratio of about 1.7, based on figure 4. The hybrid device offers a considerable improvement. Actual test results on a hybrid flow limiter are given in the next section. The device tested was a prototype which was not optimized. It produced a mass flow ratio of 1.3, compared to a ratio of 1.83 measured with an orifice type contraction-expansion restrictor.

Experimental performance.- Several flow restrictors, including orifices, venturis, vortex valves, and a hybrid-fluidic controller, have been studied experimentally to determine their characteristics as flow limiting devices. Testing was conducted on a flow bench (shown in figure 8) suitable for evaluating the low flow rates of liquid water to be expected with biowaste resistojets. Flow meters seen in the center of the flow bench control panel cover the range 0.002 to 9 grams per second. Typical water mass flow rates for a 25-mlb biowaste resistojet are from 0.04 to 0.08 grams per second, depending on chamber temperature. Final miniaturization of the flow limiting

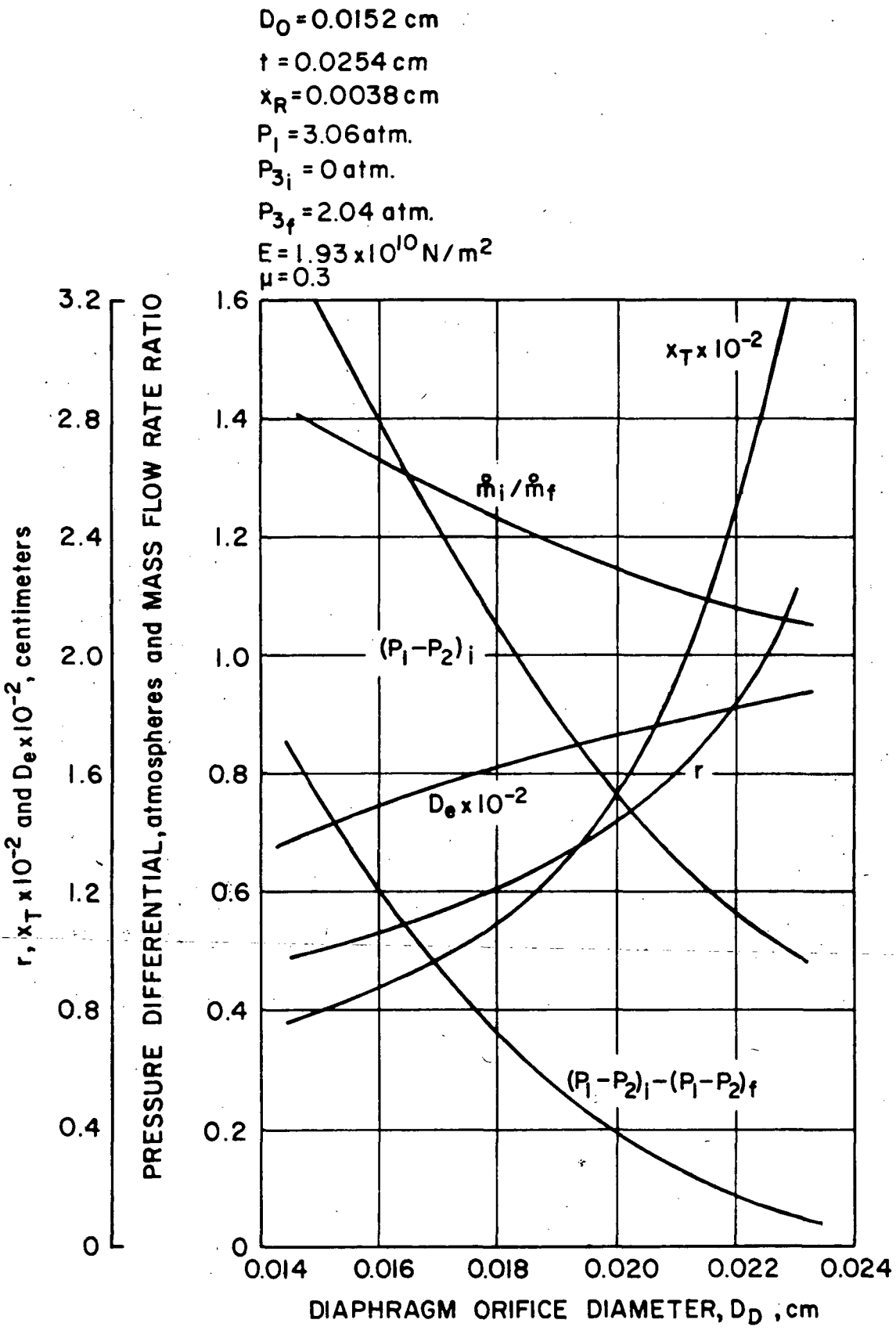

Figure 7.- Hybrid flow limiter predicted performance.

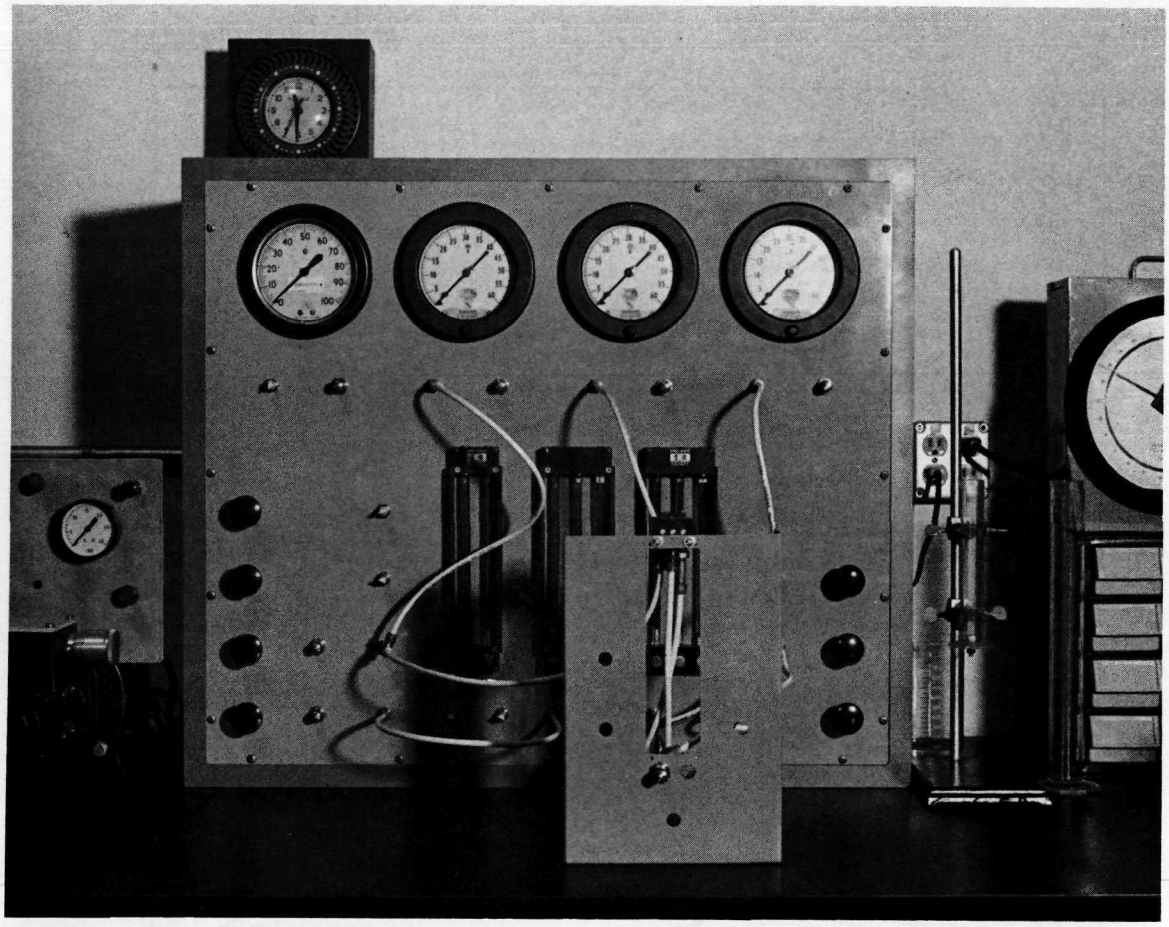

Neg. 125-3

Figure 8.- Fluid flow bench.

devices was not undertaken and these tests include flow rates to as low as 0.06 grams per second. The objective of these tests was to evaluate feasibility of candidate flow limiting concepts in sizes sufficiently small to approximately correspond to the flow regimes, delay times, etc., pertinent to an actual application flow condition.

Referring to figure 2 for water flow initiation to a resistojet in space, there would be a hard vacuum condition downstream of the shut-off valve. An initial increment of water would flash to vapor and would affect the starting dynamics. The flashing to vapor would be beneficial to the achievement of steady-state conditions by increasing the rate of pressure buildup to operating chamber pressure. The two-phase flow effects were not included in the experiments discussed in this report. Flow characteristics were evaluated in terms of pressure drop, which, for incompressible flow devices, is independent of the absolute pressure level. Testing to include the actual hard vacuum starting environment should be included when the final selected flow limiting concept is studied in detail for actual incorporation into a thrustor design.

Table II lists the fixed geometry flow limiter configurations tested. Included were five small diameter orifices and nine vortex valve configurations. Three of the orifices (configurations E, F and G) were molded plastic precision orifices made by Johnson Service Co., Milwaukee, Wisconsin and used in fluidic circuits. The smallest orifice tested (configuration N) was made by drilling through a 0.025 cm thick plate with a number 97 twist drill. This orifice was also tested with radial inflow by spacing a second plate 0.010 cm upstream of the orifice plate (configuration P). A larger (0.084 cm diameter configuration L) orifice was made by drilling through a 0.025 cm thick plate with a number 66 twist drill. None of the orifices are truly orifices as accepted in fluid metering practice; that is, with a plate thickness limited to 1/8 of the hole diameter (L/D of 0.125). L/D's are listed in table II and range from 0.3 to 1.7 for the tested configurations. As a result of using the relatively thick plate orifices, a small viscous loss is introduced which would shift the theoretical sensitivity of a contraction-expansion device from 0.5 toward 1.0, corresponding to a laminar conduit device.

The vortex valve tested was a modified General Electric VC-13 non-vented vortex valve. This valve can be seen in the foreground in figure 8 as a black block on top of the sheet metal mounting stand. The stock VC-13 vortex valve is comprised of a stack of 14-0.010 cm thick-photoetched-corrosion resistant steel shims. Each shim has a vortex chamber of 1.22 cm diameter with four radial supply channels and two tangential control nozzles. The vortex shim stack is bounded on the top and bottom by blank shims having 0.23 cm diameter holes serving as flow sinks. The effective flow nozzle size of the stock vortex valve is 0.24 cm diameter; much too large for the intended flow limiting requirements. The valve is non-vented in that all input supply and control flow leaves as the output flow. For these tests, the vortex valve was modified by removing some of the shims and substituting smaller sink hole sizes to result in a flow reduction factor compared to the stock valve of as much as 60.

Figure 9 presents flow performance data for several orifice restrictors and vortex valve configurations tested, plotted on log-log scales. This is convenient in that the local slopes of the performance curves are equal to the sensitivity n as defined in equation (18). Thus, devices with the least

TABLE II

FIXED GEOMETRY FLOW LIMITER CONFIGURATIONS TESTED

Config.	Type	Restrictor* Diameter cm	Vortex Depth cm	Sink Flow Area cm^2	Orifice Length to Diameter Ratio	Entrance to Orifice Diameter Ratio
A	Vortex	.023	.010	$.55 \times 10^{-2}$	-	-
B	"	.036	.020	$.89 \times 10^{-2}$	-	-
C	"	.043	.030	1.21×10^{-2}	-	-
D	"	.053	.051	1.43×10^{-2}	-	-
E	Orifice	.025	-	-	1.0	3.0
F	"	.043	-	-	0.6	3.47
G	"	.066	-	-	0.4	2.32
H	Vortex	.025	.010	$.77 \times 10^{-2}$	-	-
I	"	.035	.020	$.55 \times 10^{-2}$	-	-
J	"	.061	.081	1.98×10^{-2}	-	-
K	"	.053	.051	1.98×10^{-2}	-	-
L	Orifice	.084	-	-	0.3	**
M	Vortex	.026	.010	8.2×10^{-2}	-	-
N	Orifice	.015	-	-	1.7	-
P	Orifice	.015	-	-	1.7	***

* - Equivalent diameter based on $C_D = 0.65$ for vortex valve configuration.

** - In this test, a small .084 cm diameter sink was used with full vortex valve depth (0.142 cm) to affect an orifice restriction.

*** - In this test, flow into the orifice was radial between the orifice plate and a parallel plate forming a .010 cm thick spacing.

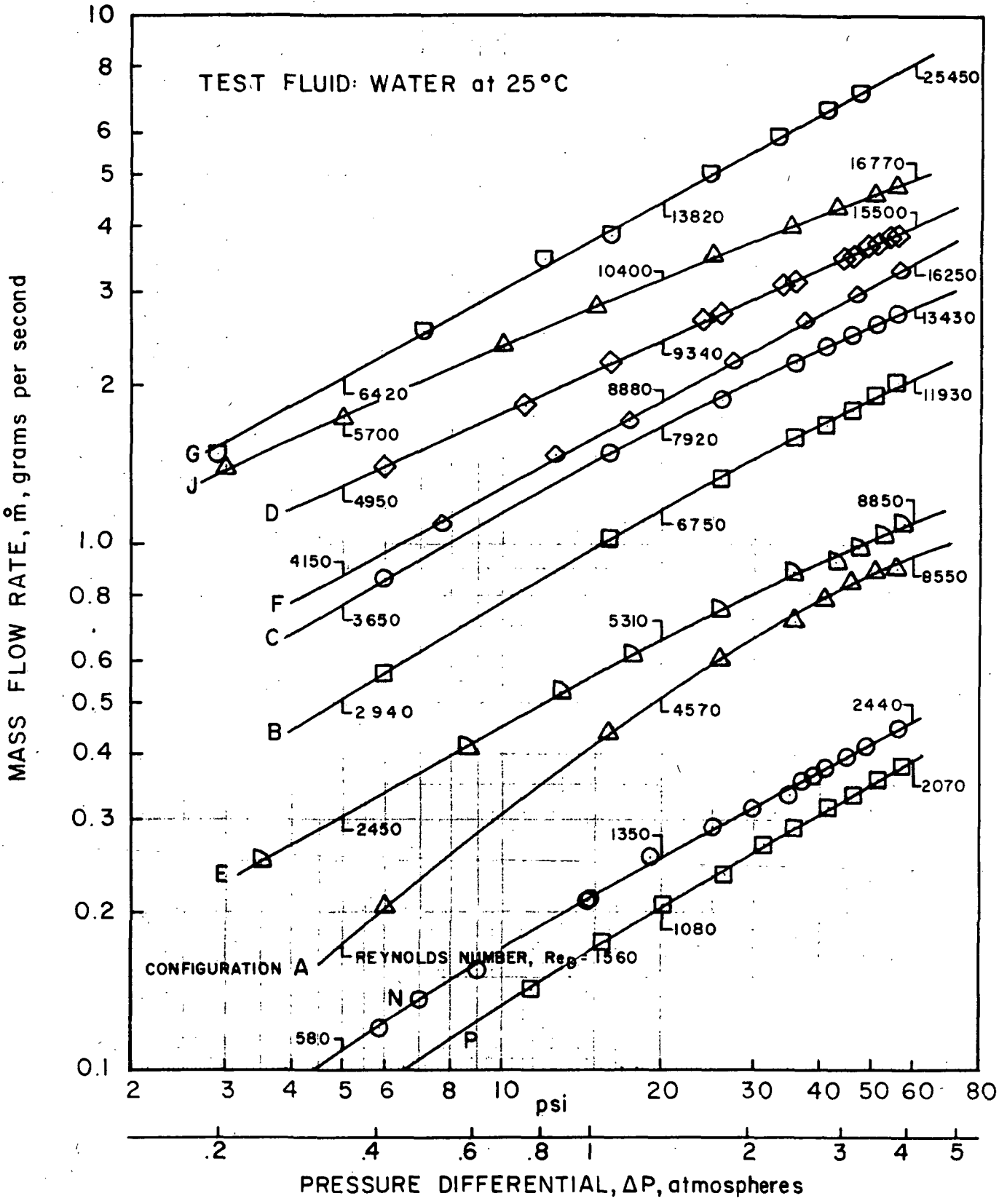

Figure 9.- Flow restrictor performance.

slope offer the best flow limiting. Reynolds numbers are indicated on the figure 9 curves at pressure drops of 5, 20 and 60 psi. The Reynolds numbers are based on the orifice diameters in the case of orifice restrictors. In the case of the vortex valve, flow restriction results from the series arrangement of the control parts and outlet sink holes. An effective restrictor diameter based on mass flow rate, pressure differential, and a discharge coefficient of 0.65 (an arbitrary value) was used to calculate the Reynolds numbers for the vortex valve configurations.

For the orifices, laminar flow should persist within the orifice, even for Reynolds numbers above 2000-2300 (the upper limit for laminar flow in tubes having fully developed flow). Insufficient flow length is available for fully developed flow. Approach Reynolds number is negligible for the configuration L and N orifice. For the configuration E, F, and G orifices, the entrance-to-orifice diameter ratios are listed in table II, indicating Reynolds numbers in the entrance to the orifices of about 1/3 those in the orifice proper. In the flow range of interest (of the order of 0.1 gram per second), laminar flow conditions exist and viscous effects introduce an influence on the overall flow sensitivity corresponding to laminar conduit flow (n equal to unity). An evaluation of entrance Reynolds numbers is complicated in the vortex valve by the vortex spin-up and a clear definition where the actual restriction occurs. Generally speaking, the control ports through which flow was introduced into the vortex chamber are small high velocity-high L/D nozzles, suggesting the introduction of turbulent wake into the vortex chamber. This is probably damped before reaching the sink hole. For configuration A at least, with a flow depth of only 0.010 cm, laminar flow probably persists everywhere in the vortex valve restrictions (control nozzle and sink hole).

Table III compares slopes or sensitivity of $\mathring{m}$ to ΔP, taken from the low ΔP and high ΔP ends of the curves in figure 9. The highest flow vortex configuration tested - configuration J - had the least sensitivity of all of the configurations tested. That is, it had the lowest value of n at each ΔP region, as compared to the other configurations with a slope of 0.40 at the high ΔP end and 0.45 at the low ΔP end. This indicates that vortex action does offer improved flow limiting characteristics compared to a simple fixed restrictor (orifice or nozzle). Referring to the sensitivities given in table III for configurations J, D, C, B, and A in order of decreasing vortex effective size, the trend is toward increased sensitivity.

An otherwise large flow rate - very high Reynolds number vortex valve - was scaled down in thickness while maintaining the spin chamber diameter constant. Most likely, as configuration A and B for instance, the tested vortex valve is non-optimum having a spin chamber very thin relative to its diameter. In a flow size compatible with the 25-mlb resistojet, it is anticipated that viscous effects in the vortex chamber will predominate and sensitivity will not be significantly lower than that of a simple fixed restrictor.

Recalling that theoretical sensitivity shifts from 0.5 for a contraction-expansion device to 1.0 for a laminar conduit device, we see that the numerical trend is consistent with the data of table III. Slopes are greatest at the low flow = low ΔP - lower Reynolds number end in all cases. The large size - high Reynolds number orifice configurations F and G exhibited linear characteristics, or constant sensitivities, of about 0.55, close to the theoretical value for

TABLE III

FLOW SENSITIVITY OF TYPICAL FLOW RESTRICTORS

Configuration	Pressure Differential Region	Slope, n
A	Low	0.80
A	High	0.55
B	Low	0.60
B	High	0.50
C	Low	0.58
C	High	0.45
D	Linear	0.45
E	Low	0.56
E	High	0.45
F	Linear	0.56
G	Linear	0.55
J	Low	0.45
J	High	0.40
N	Low	0.66
N	High	0.54
P	Low	0.66
P	High	0.56

the contraction-expansion device. The 0.55 sensitivity value indicates a contraction-expansion value of 0.50 with some superimposed viscous (laminar conduit) effects. The 0.45 sensitivity for the high ΔP value of configuration E is apparently a matter of resolution of the data. The smallest orifices, N and P, indicate additional viscous effects with a mean sensitivity of about 0.6. Scaling down to the flow requirement of a 25-mlb resistojet, viscous effects would be more predominate and a sensitivity of about 0.7 is likely with a fixed contraction-expansion device.

The vortex valve configurations were also tested as true fluidic vortex throttling valves. Flow was introduced into the normal supply ports and the turn-down characteristic was documented as control port flow was introduced. Typical data are shown in figure 10 where the total output mass flow rate at constant supply and output pressures is seen to decrease for configurations B and C as control flow is increased (represented by an increase in control pressure). No turn-down resulted with vortex valve configuration A, comprised of only one 0.010 cm thick shim. While the total output flow increased slightly from 3.39 to 3.49 grams per second for the data of figure 10, the supply flow decreased from 3.39 to 2.76 grams per second with increasing control pressure (flow). The data of the valve is such that, for constant supply pressure and output pressure, the vortex chamber flow may or may not spin-up to effect a reduction of supply flow. If the sink presents the major flow resistance, then with both supply and control streams competing for the sink with ΔP across the sink held constant at

$$\Delta P_{SINK} = P_S - P_{out} = 30 - 4 = 26 \text{ psi},$$

the supply flow necessarily must throttle back as control flow is inputted. Since a substantial turn-down ratio was observed with twice the number of shims (configuration B) it is likely that some degree of spin-up was evident in configuration A also.

The data of figure 10 are not specifically related to the flow limiter problem. These data are presented as a matter of interest to those engaged in fluidic systems technology. The units of psig for pressure are used for convenience in comparing the vortex valve performance against manufacturer's (GE) data sheets.

When the vortex valve is operated as a flow restrictor (data of figure 9), supply flow is zero and all flow is inputted via the control nozzles (tangential to the vortex chamber). For this case, a significant spin-up in the chamber is to be expected even for the single shim configuration A. Comparing the high pressure drop region sensitivities in table III for configurations A (smallest vortex) and E (smallest orifice), it appears that the configuration A vortex valve behaves essentially like an orifice at the high flow end. At the low flow end, it appears configuration A behaves much like an orifice with a significant viscous loss factor, by virtue of its 0.80 value of sensitivity, which approaches the theoretical laminar restrictor value. In order to verify that configuration A flow was not predominately controlled by the sink hole size used, configurations H and M were run with the same single vortex shim but with considerably larger sink areas. Flow performance was essentially unchanged from that for configuration A, demonstrating that the flow resistance was

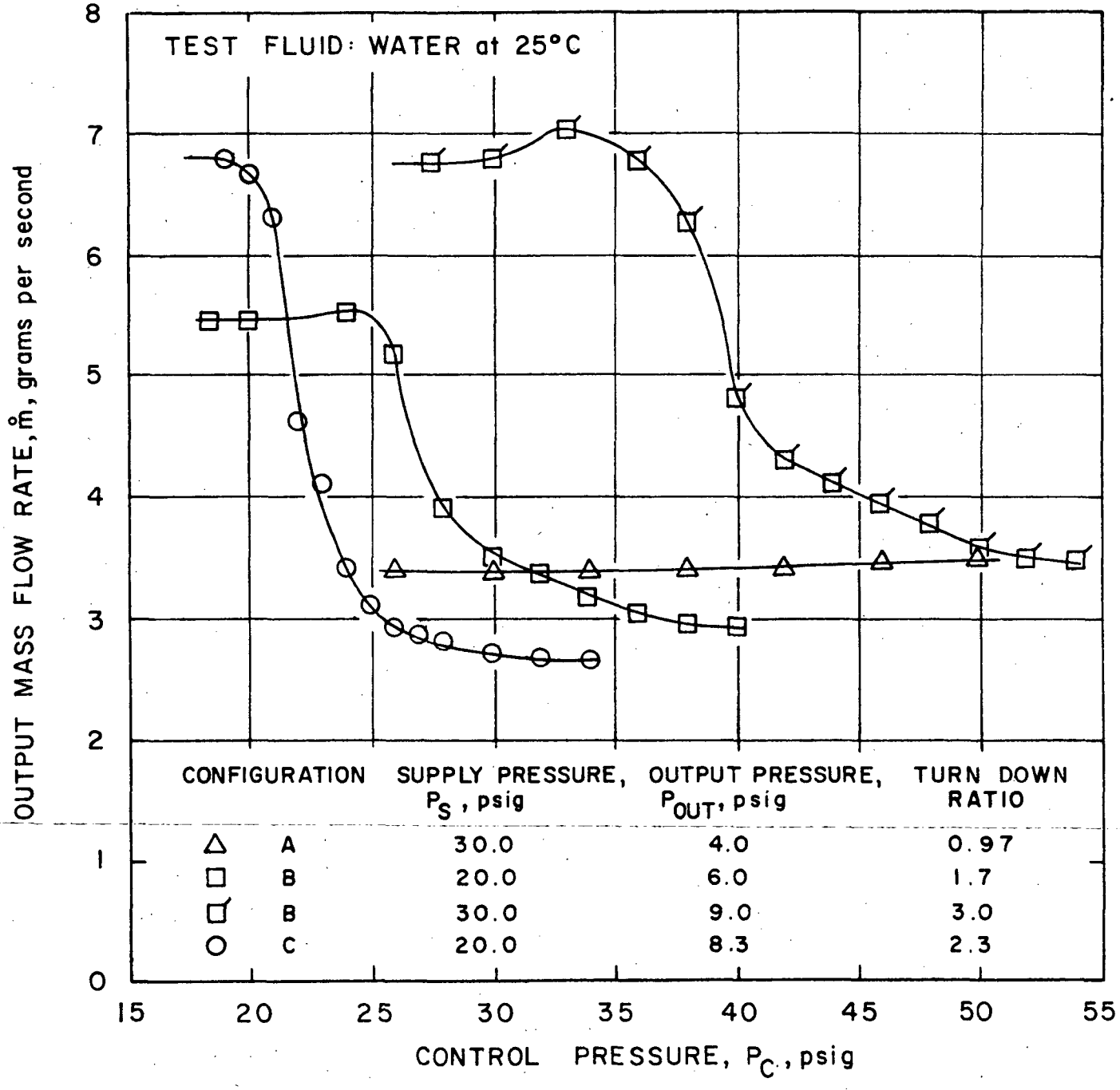

Figure 10.- Vortex valve performance.

essentially that of the vortex chamber control nozzles. Comparing the higher Reynolds number configurations D (vortex) versus F and G (orifices), it appears that the vortex valve used as a flow restrictor results in 80% of the sensitivity of the simple orifice restrictors. For smaller configurations but also high Reynolds numbers (c.f. the high ΔP end of the curves for configurations A and E), the vortex valve shows no advantage over the orifice restrictor. Scaling across curve A to E to compare slopes at about the same Reynolds number, it appears that the orifice restrictor is less sensitive.

It should be emphasized that a large flow rate - very high Reynolds number vortex valve - was scaled down in thickness while maintaining the spin chamber diameter unchanged. Most likely, as configuration A and B for instance, the tested vortex valve is non-optimum. Additional testing would be required at lower Reynolds numbers approaching those of the actual flow limiter/biowaste resistojet application in order to assess the true capability of the vortex valve for the intended application. For example, the vortex valve, and more specifically the spin chamber, should be scaled down to effect a more optimum spiral path relative to the viscous effects which start to become predominate at the Reynolds numbers of interest. Considering a 25-mlb biowaste resistojet with a specific impulse of 250 seconds as an example, a mass flow rate of 0.045 gram per second is indicated. This required scaling down by a factor of about 4.5 from the lowest vortex valve flow data of figure 9. Effective flow restrictor size will decrease to about 0.0075 cm, a factor of 2 smaller than the smallest configurations (orifices) discussed in this report. As with orifices N and P (see table III), viscous effects will become important causing significant increases in the sensitivities. In this respect, further development of the vortex valve for the 25-mlb resistojet flow rate does not appear to offer an improvement over the simpler orifice restrictor.

While not specifically relevant to the flow limiting problem, it is valuable to other fluidic applications to note that a factor of 7 reduction in the GE VC-13 vortex valve depth was accomplished, resulting in a useful turn-down ratio of 3.0 (configuration B at 30 psig supply pressure). The reduction in power consumption (i.e., mass flow rate) for this case relative to a stock VC-13 vortex valve was a factor of 63.

Three small venturis were fabricated having throat diameters of 0.015 cm and divergence half angles of 11° and 15°. Ultrasonic excitation was tried on the venturis and on one of the orifices tested to induce cavitation. An ultrasonic generator operating at 21KHz with a total output power of 80 watts and an output power density of 0.4 watts per square centimeter was used. The flow fittings were pressed against the generator transducer output plate. While the power level within the flow restrictors could not be measured, it is believed sufficiently strong to induce cavitation in otherwise marginal flow situations.

To evaluate qualitatively the effect of the ultrasonic energy on small flow streams, orifices of various sizes were free-jetted in a water bath exposed to the transducer. Faint clouds of minute bubbles were visible in the free jets from orifices having throat diameters of 0.025 to 0.050 centimeters. Typically, the minute bubbles formed a core about 0.4 cm long which stood off from the exit face of the orifices about 0.1 cm. With the smallest orifice, the clouds were barely visible and were intermittent.

Flow data taken on the venturis and one orifice plate 0.015 cm in diameter by 0.025 cm long revealed no throttling due to cavitation, with or without excitation. On the contrary, under most flow conditions, small (of the order of 2 percent) flow increases occurred when the excitation was applied. The ultrasonic excitation appeared to have reduced the viscous boundary effects. The faint clouds observed in the free jet tests may have been outgassing. In any case, these clouds are believed to contain very minute bubbles and did not have the appearance of a vigorous active cavitation core.

Pressure differentials of up to 4.7 atmospheres were applied to the cavitating venturis, resulting in values of the cavitation parameter from equation (20) as low as 0.1. The tests conducted are considered preliminary since only a few geometries were evaluated. Since delay time is an important factor in cavitation and particularly so in the miniature size venturies tested, perhaps long throat sections would result in cavitation. The 0.015 cm throat size venturis are difficult to fabricate without causing what may amount to significant discontinuities at the throat-to-diffuser intersection. Therefore, it may be possible under ideal conditions to throttle by cavitation in such small venturis. It is very likely, however, that performance repeatability would become a problem. In general, it appears that the miniature cavitating venturi is not a suitable candidate for a flow limiter for the biowaste resistojet.

Figure 11 shows an assembled and disassembled prototype of the hybrid flow limiter. This unit was fabricated using the analytical criteria presented in figure 7 of the previous section as a guide. In the foreground of the disassembled view the backing plate, the orifice plate and the diaphragm can be seen (refer to figure 6 for relative placement of the elements in the flow limiter). Two 0.206 cm (0.081 inches) diameter holes can be seen in the backing plate. Not visible are two 0.0152 cm (0.006 inches) diameter holes in the orifice plate and one 0.020 cm (0.0079 inches) diameter hole in the diaphragm. The off-center holes (per figure 6) were located 1.04 cm (0.4 inches) off-center.

Next to the two body halves in figure 11 are four typical spacers. These were fabricated with internal radii (r per equation 37) of 1.52, 1.40, 1.27 and 1.14 cm. Each of these internal radius-sized spacers were made in thicknesses of 0.0053, 0.0078, 0.0109 and 0.0132 cm. The diaphragm was made from 0.0254 cm thick corrosion resistant steel shim stock. With this variety of spacer sizes, the effects of radius and spacer thickness could be evaluated.

The off-center holes in the diaphragm and orifice plate are located part way out along the spacer radius r. The spacer radius r can be seen in figure 6 to set the effective working radius of the diaphragm*. The off-center holes, then, are partially influenced by the diaphragm motion, unlike

---

* An additional variation relative to the analytical model occurs in the constraint on the diaphragm. The upstream body half has an internal radius of 1.52 cm. Therefore, when using the smaller radius spacers, the diaphragm working radius is effectively slightly larger. This was done for convenience in making the prototype unit.

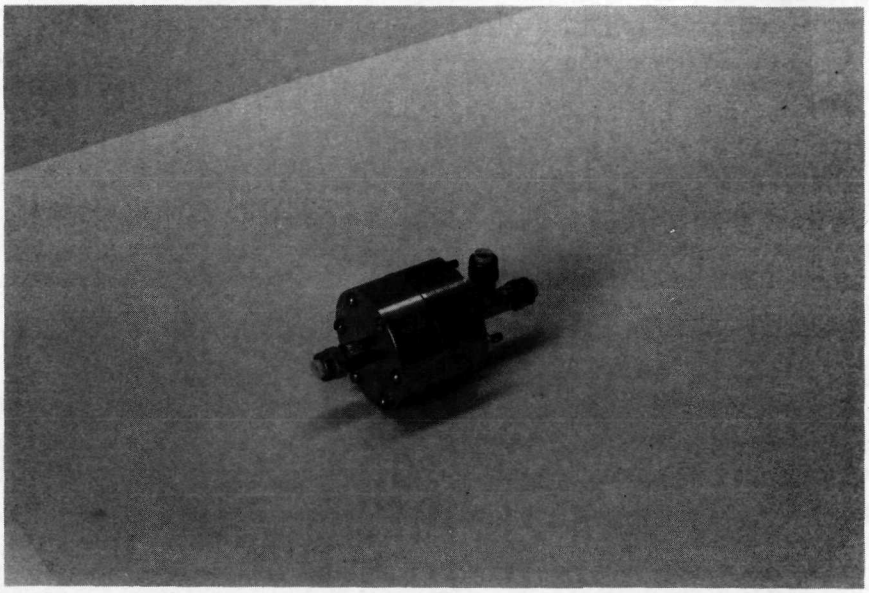

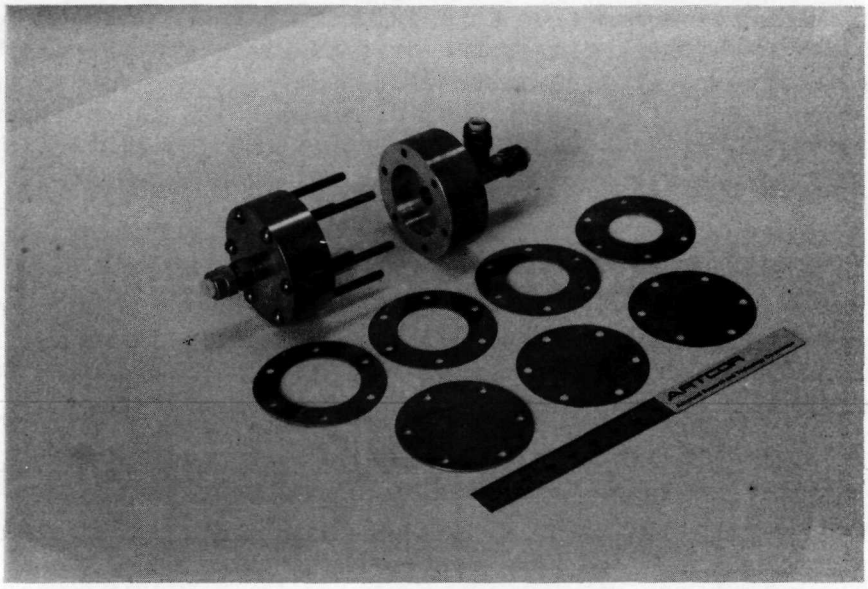

Figure 11.- Hybrid flow limiter prototype hardware.

the assumption made in deriving the figure 7 analytical performance. The consequence of this is not significant. This point is made, however, since an insufficient off-center distance could result in erratic performance. To comply with the analytical model assumptions, the off-center orifices can be recessed in counter bores away from the intermediate space 2 in figure 6.

The prototype was operated with two relative orientations of the off-center holes. In one case, the diaphragm hole was located directly over the off-center orifice plate hole. Here the interaction of the off-center holes with diaphragm deflection is eliminated. However, the diaphragm hole exhaust jet is impinging into the off-center orifice plate hole effectively tending to make the orifice plate hole larger. That is, it passes more flow than it would if its input flow was derived from a quiescent condition in the intermediate space 2 (figure 6) away from the diaphragm hole exhaust jet. In the other case, the off-center holes were displaced 180 degrees.

Figure 12 presents typical data taken on the figure 11 hybrid flow limiter. A long hole type fixed orifice restrictor calibration curve (circle symbols) is shown for reference purposes. This fixed orifice had a 0.0152 cm (0.006 inches) diameter hole with a length of 0.0254 cm (0.010 inches). Using a total spacer thickness of 0.0230 cm, the uppermost curve (diamond symbols) was obtained to show the effective flow size of the hybrid flow limiter without diaphragm deflection action. Ratioing the mass flows at a given pressure differential from figure 12, the hybrid flow limiter orifice arrangement is effectively 50% larger than the fixed orifice. The S-shaped curves in figure 12, for which throttling of the center orifice is occurring, indicate that the throttled hybrid flow limiter is effectively smaller in size than the fixed orifice restrictor.

One curve is shown (open triangular symbols) for the case where the off-center orifices are aligned. The solid symbol data in figure 12 are for the case of these holes displaced 180 degrees. From the triangular symbol data (open and solid) the effect of diaphragm hole impingement on the off-center orifice plate hole is seen. In the range of diaphragm interaction (deviation from a fixed restrictor trend) the case of displaced holes is seen to result in less sensitivity of mass flow to pressure drop. Finally, the three curves of solid symbol data indicate how performance is shifted with changing spacer thickness. The curves can be shifted left or right by using larger or smaller spacer radii. In this way, the hybrid flow limiter can be optimized for a particular biowaste resistojet application. The curves are also shifted with spacer thickness; for example, a thicker spacer delays center orifice closing to a higher pressure differential.

Taking, as a typical case, a thrustor supply pressure of 3.06 atmospheres (45 psia) and a chamber pressure of 2.04 atmospheres (30 psia), the data of figure 12 can be compared. The pressure conditions correspond to an initial pressure differential of 3.06 atmospheres (45 psia) decreasing to a final pressure differential of 1.02 atmospheres (15 psia). Table IV compares the initial to final mass ratios for these typical pressure conditions and for the data of figure 12. In effect, the data have been normalized and do show the relative improvement in mass flow limiting offered by the hybrid device. The pressure differential range chosen for comparison is arbitrary and does not reflect optimums in terms of minimum mass flow rate ratios. Shifting the

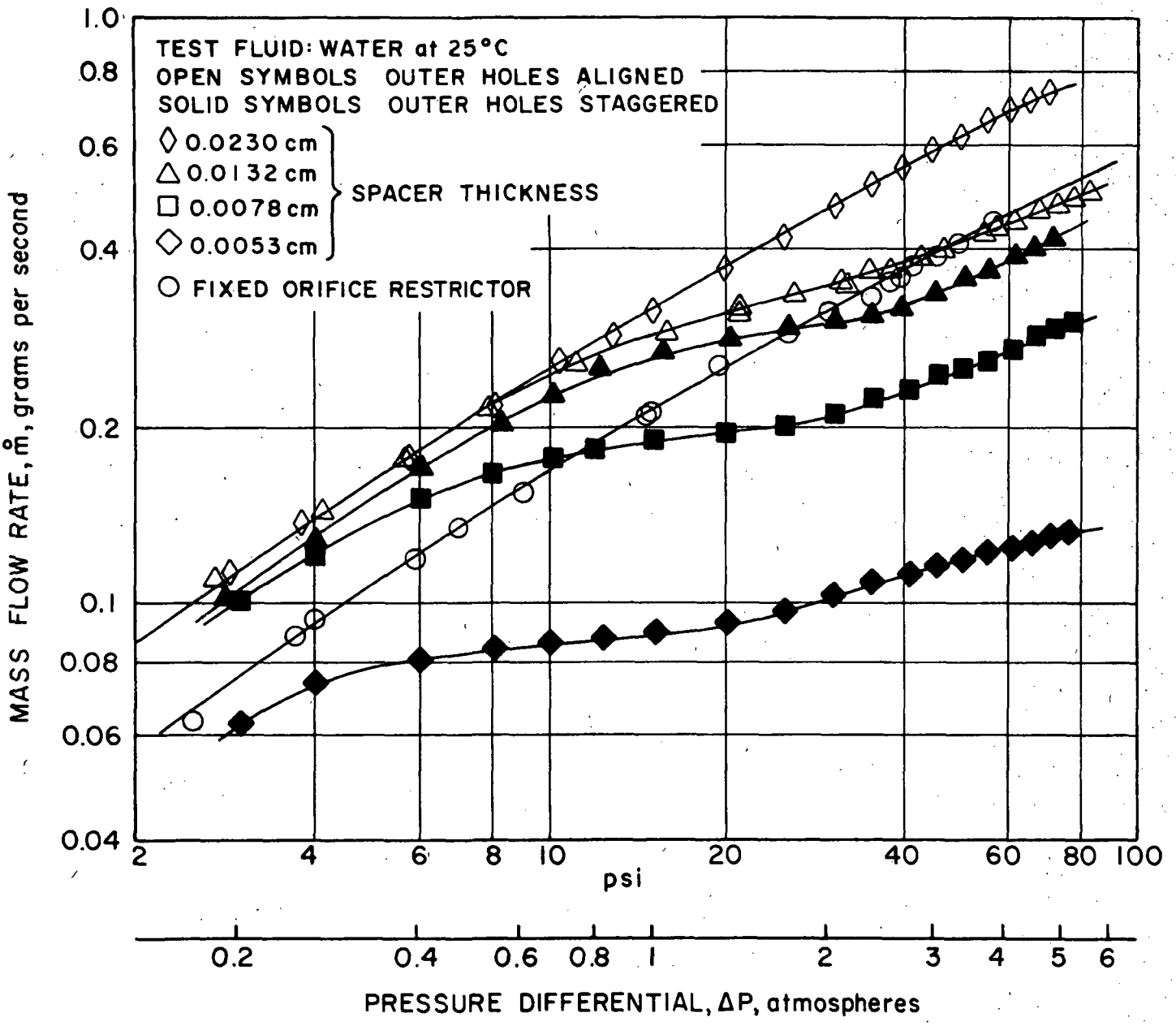

Figure 12.- Hybrid flow limiter performance.

curves to the right in figure 12 would yield lower mass flow ratios, for example. Table IV also includes values of sensitivity n (see equation 18) taken between the 3.06 and 1.02 atmosphere points along each curve. While the orifice demonstrates a sensitivity of 0.56, the hybrid flow limiter shows considerable improvement at 0.22.

TABLE IV

HYBRID FLOW LIMITER PERFORMANCE

Device	Figure 12 Symbol	Spacer Thickness cm	Initial to Final Mass Flow Rate Ratio, $\dot{m}_f/\dot{m}_i$	Sensitivity, n
Fixed Orifice	○	-	1.83	.56
Hybrid - No Diaphragm Action	◇	0.0230	1.85	.56
Hybrid	△	0.0132	1.33	.30
Hybrid	▲	0.0132	1.29	.23
Hybrid	■	0.0078	1.27	.22
Hybrid	◆	0.0053	1.30	.24

For all the hybrid flow limiter data presented in figure 12, a 1.4 cm (0.55 inches) spacer radius r was used. The effective value of r is slightly larger than that because of the inlet end body radius effect. Referring back to the analytical interpretation of the hybrid flow limiter performance in figure 7, a diaphragm orifice diameter D_D of 0.020 cm (0.0079 inches) indicates that a mass flow rate ratio of 1.15 would occur and that a spacer internal radius r of 1.44 cm should be used. A total deflection x_T of 0.0154 cm is indicated, suggesting the spacer thickness to be used. For the thickest spacer fabricated (0.0132 cm) and used in the test, a mass flow rate ratio of 1.29 (solid triangular data) resulted. Had a slightly thicker spacer, say 0.0154 cm thick been used, the solid triangular data curve of figure 12 would have moved to the right and, for the pressure differential range used to interpret mass flow ratios in table IV, a lower mass flow ratio would have resulted. The same effect could be obtained by using a larger spacer radius to increase the diaphragm working area.

It appears that the hybrid flow limiter performance can be predicted with sufficient accuracy to make the hybrid concept a readily usable device. A more rigorous analytical treatment (involving equation 39) and elimination of diaphragm deflection interaction with the off-center holes should bring the analysis and experimental performance into close agreement. Using photo etching techniques, the critical parts of the hybrid flow limiter (diaphragm and orifice plate) can be fabricated with sufficient accuracy to obtain a high

degree of performance repeatability between assemblies. The mass flow rate ratio obtainable with the hybrid device can be tailored to match dynamic requirements of the biowaste resistojet. In this respect, the mass flow rate ratio of the simpler contraction-expansion device may also be suitable. These devices - both hybrid and fixed geometry configurations - offer a range of mass flow rate limiting capability which can be used to optimize the transient performance of the thrustor and provide safe and reliable start-up characteristics with liquid water propellant.

THERMAL PUMPS

General Considerations

Thermal pumps were studied as possible replacements for the mechanical pumps being considered on the baseline space station for desorption of the molecular sieve of its CO_2. A cyclic-constant volume cryopumping concept appears attractive for this function using radiation to dark space for a heat sink and using the space station as a heat source. Figure 13 presents the model being considered using, for typical parameters, the baseline molecular sieve specifications per reference 11.

The baseline CO_2 system includes two mechanical pumps. All of the molecular sieve desorbed CO_2 is pumped to an intermediate storage vessel at a pressure of 2 to 3 atmospheres. Sixty percent of the desorbed CO_2 flows to the Sabatier reactor for conversion to oxygen and 40 percent is available as resistojet propellant. This propellant is pumped by a second pump to the propellant storage tanks having a maximum pressure of 20 atmospheres. Three thermal pumping configurations were considered sufficiently attractive for trade-off studies:

(1) Utilization of two separate thermal pumping systems to replace the baseline mechanical pumps.

(2) One thermal pump which pumps the entire molecular sieve desorbed CO_2 to the 20 atmosphere propellant storage tanks with a pressure-regulated return from the propellant storage tanks to the intermediate storage tanks.

(3) Thermal pumping between the molecular sieve and intermediate tank only with mechanical pumping of the propellant to the propellant storage tanks.

Configuration (3) was considered in case thermal pumping to the 20 atmosphere level was found to be impractical. This option is still attractive from a power consumption point of view since the low pressure mechanical pump requires 75 percent of the total CO_2 pumping power requirement.

As indicated in figure 13, two molecular sieves are used and desorbed alternately on one-hour cycles. While one sieve is being desorbed for 30 minutes, the other is adsorbing for 30 minutes. The molecular sieve output is 12 Kg of CO_2 per day. Exposed to space, the cryopump solidifies CO_2.

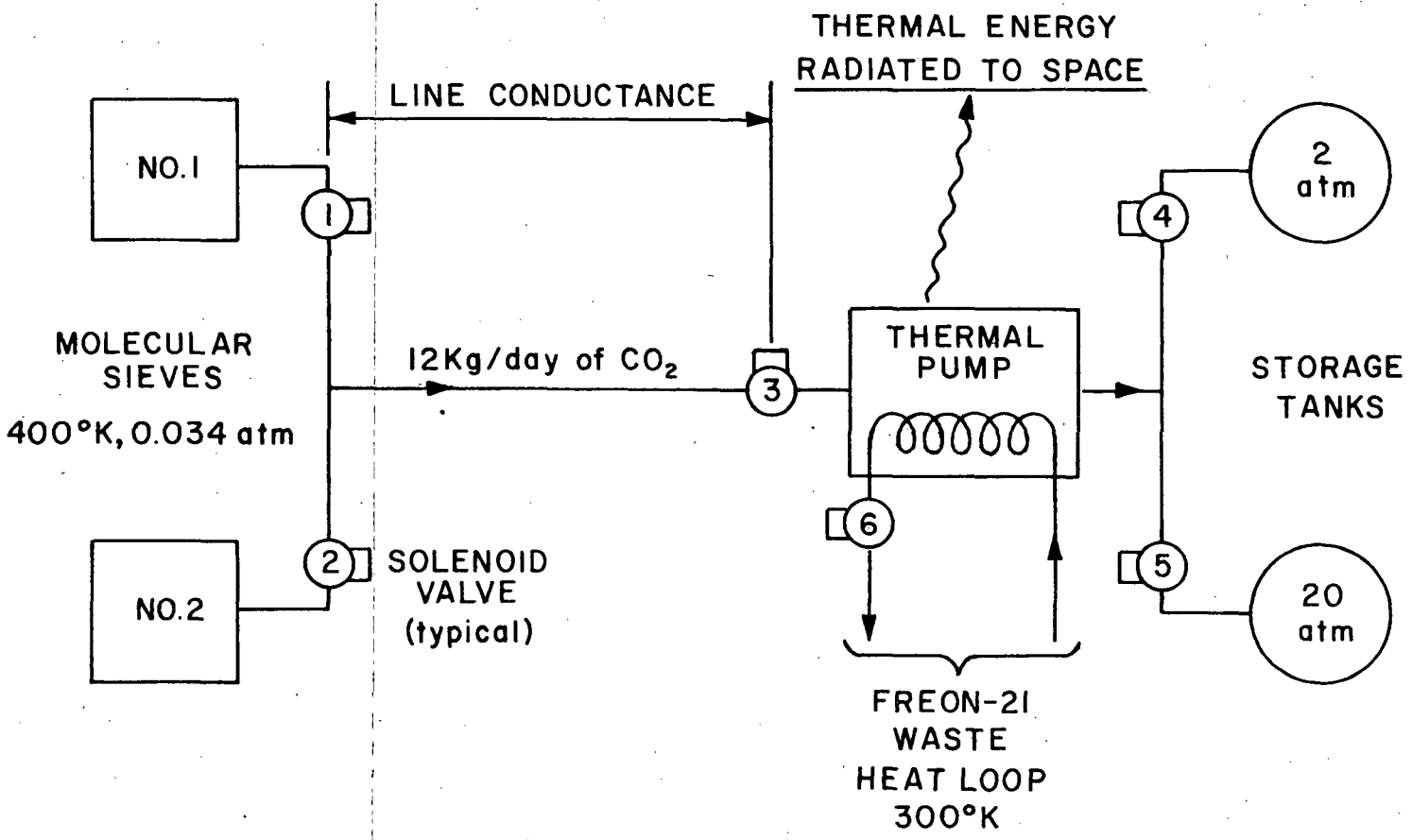

Figure 13.- Thermal pump model.

By valving off the molecular sieve and valving into the storage tank through check valves, subsequent heating with phase change results in pressurization and a transfer of the CO_2 to the storage tanks.

The cryopump is divided into four sections with each section occupying a quadrant in order to have a dark side exposure available for the cryotrapping portion of the cycle. The cryopumping system involves a significant weight penalty compared to a mechanical pumping system, but offers the following advantages:

(1) Negligible electrical power consumption relative to mechanical pumps.

(2) The bulk of the pump weight is in the space radiators which effectively serve to dump spacecraft waste heat. In this respect, the radiators supplement or replace a portion of the normal waste heat radiator system.

(3) The cryopumping system could be developed to pump a variety of fluids serving other than the resistojet propulsion system requirements.

(4) In the case of pumping of desorbed CO_2, some oxygen is transferred from the sieves. It may be possible to vent a good portion of this oxygen during the cryotrapping, permitting higher temperature operation with the resistojets.

Water and Freon waste heat loops are available for heating the thermal pump. In cryotrapping CO_2, however, temperatures to 162°K are reached which would present a freezing problem with the water. The figure 13 model depicts Freon-21 at about 300°K to heat the pump for pressurization of the CO_2 into the storage tanks. Storage tank pressures from 2 to 20 atmospheres were considered in this study per the baseline system requirements.

During cryotrapping, either valve 1 or 2 and valve 3 are open (see figure 13). Valves 4 and 5 are closed. The molecular sieve being desorbed is heated to about 400°K. CO_2 passes to the thermal pump at a pressure of 0.034 atmospheres (0.5 psia). Since the sieves may be located some distance from the pump and because of the low density at 400°K and 0.034 atmospheres, line conductance effects can be important and are evaluated in the next section. Cryotrapping occurs with a dark side exposure on the radiator being used and with valve 6 closed to prevent the introduction of waste heat. To pressurize and pump CO_2 to the storage tanks, valve 3 is closed and valve 6 is opened, as is either valve 4 or 5, depending on which tank is to receive CO_2.

It would be possible to shutter off the pump to space to minimize its heat loss by radiation to effect a minimum heat-up time. This is not considered practical and, fortunately, is not necessary. The waste heat input overwhelms the cooling rate and overall pump cycle time is not greatly affected.

Detailed calculations for the thermal pump are presented in the next sections. These show feasibility of the pump concept; however, practicality relative to mechanical pumps is doubtful at this time in view of the following:

(1) Large radiator areas relative to small gas side volumes necessitate long, slender gas side spaces in which blockage by maldistribution in the cryotrapped CO_2 is very likely.

(2) Using a state-of-the-art value of radiator specific mass, the cool down time for the radiator is found to be long relative to sieve desorb cycles. For example, on the order of 50 minutes chill time is required relative to a 30-minute desorb cycle requirement. This necessitates desorbing multiple sieve loads with less frequent pumping phases. In this way the chill time is amortized for an effective cycle time of 30 minutes. The actual overall pump cycle time may be of the order of 100 minutes. This becomes a potential problem in that the pump may not be in a dark side exposure for this length of time. It may be possible to match the pump cycling to dark side (desorbing) and sun side (pumping) exposure times; however, this presents an undesirable restriction on the pump concept.

Noncondensables (typically oxygen and nitrogen) may be present in the desorbed CO_2. The baseline system projects a one percent level of noncondensables. Depending on whether or not the noncondensables are cryotrapped in the solid CO_2, these could affect pump performance. In the event these remain as untrapped gas and contribute a partial pressure to the pump background pressure, periodic venting would effectively remove the noncondensables. A small mass loss would occur; however, the oxygen, undesirable for high temperature operation in resistojets having metal heaters would be removed.

The following assumptions have been made in the thermal pump cycle analysis which follows:

(1) Radiators are not shuttered; rather, they are exposed to space at all times.

(2) Radiator emissivity is in the range of 0.9 to 1.0.

(3) The effective radiator area to actual projected panel area is 1.0, a realistic value.

(4) The radiator specific mass is 4.9 Kg/m^2 (1.0 lb/ft^2), a realistic value.

(5) The pump chill time is amortized by collecting multiple sieve desorbs between pumping cycles.

(6) High pressure side gas line conductances are high relative to the low pressure side.

(7) A noncondensable mixture of oxygen and nitrogen of one percent by weight is present in the desorbed CO_2.

Thermodynamics of the Cooling Cycle

Desorption cycle time is a function of many design parameters and involves cooling of the pump. For the radiation cooling portion of the cycle, the important parameters are:

(1) surface emissivity of the radiator

(2) panel mass per unit area

The energy balance of a radiation panel at temperature T_p radiating to space (0°K) is given by:

$$\sigma \epsilon A_p T_p^4 = - \frac{m_p}{A_p} A_p C \frac{dT}{dt} \tag{40}$$

where σ is the Stefan-Boltzmann constant and is equal to 5.67×10^{-8} watt/m^2-°K^4, ϵ is the emissivity, Ap is the frontal area of the panel radiating to space in m^2, m_p is the mass of the panel in Kg, and C is the thermal capacity of the radiator material in (watt-minutes)/(Kg-°K).

The time for the panel to cool from T_1 to T_2 is found by integrating the above energy balance:

$$t = \frac{C}{3\sigma\epsilon T_{p_1}^3} \left(\frac{m_p}{A_p}\right) \left[\left(\frac{T_1}{T_2}\right)_p^3 - 1 \right] \tag{41}$$

For aluminum, C = 15.5 (watt-minutes)/(Kg-°K). To cool from T_1 = 300°K down to T_2 = 190°K,

$$t = \frac{9.81}{\epsilon} \left(\frac{m}{A}\right)_p \tag{42}$$

Note that this metal chill time is a function of the radiator panel mass per unit size. The chill time is displayed in figure 14; and it is seen that, for reasonable times, light specific weight panels are required. For a given specific weight, the chill time is independent of radiator panel size. A realistic specific weight of 4.9 Kg/m^2 (1.0 lb/ft^2) is being used for this study.

The solidification of the CO_2 will begin at about 190°K. The main energy requirement is the latent heat, which is

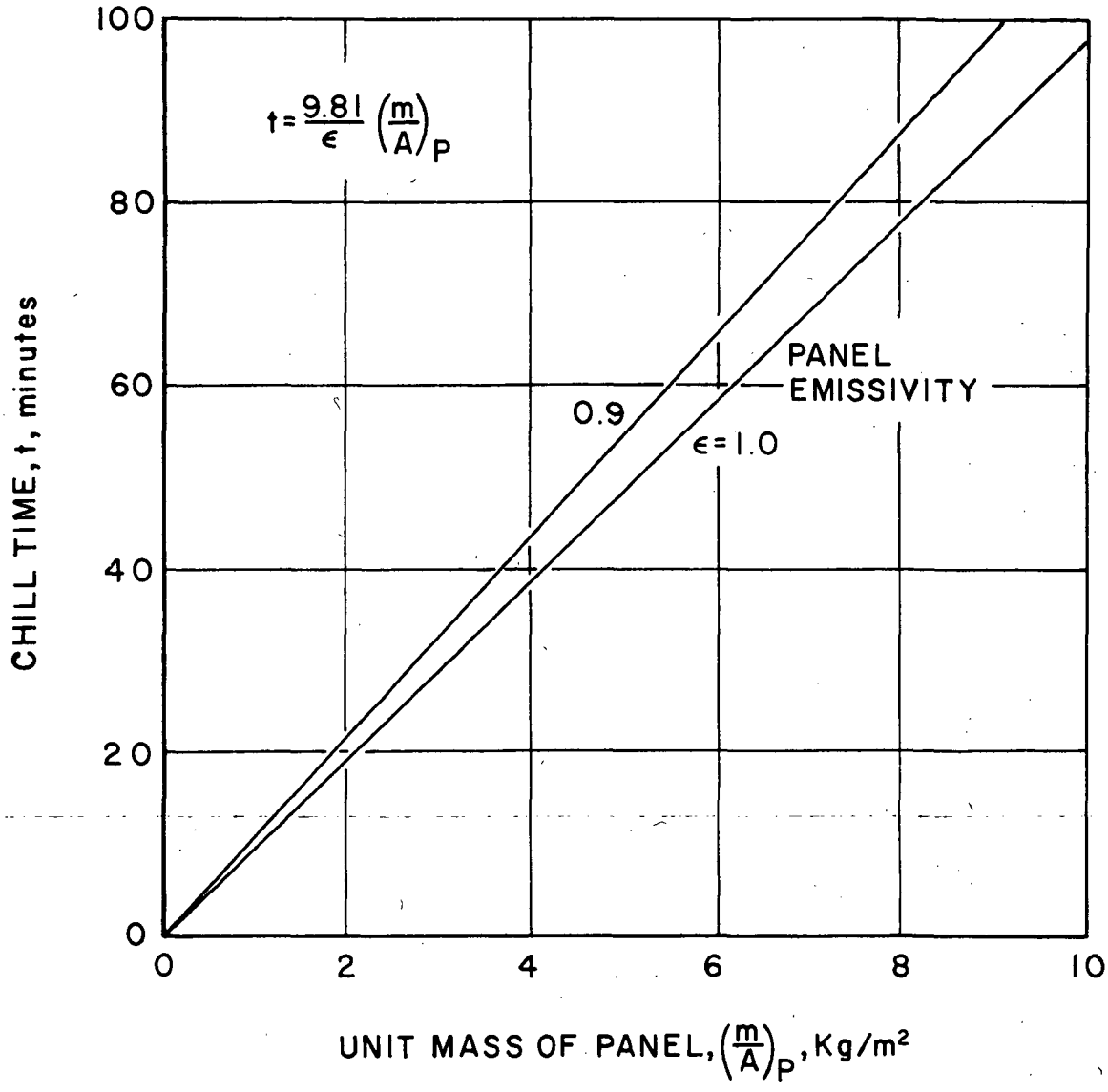

Figure 14.- Time to chill radiator panel from 300°K to 190°K.

$$L = 9660 \text{ watt-minutes/Kg}$$

Applying the cooling power to the CO_2 solidification and including the sensible heat of the CO_2 from 400°K down,

$$\sigma \epsilon A_P T_P^4 = \dot{m}_{CO_2} L(1 + \alpha) \tag{43}$$

where $\dot{m}_{CO_2}$ is the CO_2 freeze rate in Kg/min. $\alpha \simeq 0.31$ is the ratio of sensible heat (from 400°K) to the latent heat. The panel size in square meters to solidify CO_2 at 190°K becomes

$$A_P = 363 \frac{\dot{m}_{CO_2}}{\epsilon} \tag{44}$$

and is presented graphically in figure 15. Of course, the metal is also cooling during this time, and this calculation is thus a simplified representation. Considering both the metal chilling and the CO_2 freezing,

$$\sigma \epsilon A_P T_P^4 = - \frac{m_P}{A_P} A_P C \frac{dT_P}{dt} + 1.31 \dot{m}_{CO_2} L \tag{45}$$

$$\sigma \epsilon A_P \int_{T_1}^{T_2} T_P^4 dt = \frac{m_P}{A_P} A_P C (T_{P_1} - T_{P_2}) + 1.31 \Delta m_{CO_2} L \tag{46}$$

A numerical analysis could precisely accommodate the varying value of T_P from T_1 down to T_2. Here we use an average value, T_{AVG}, yielding the time as

$$\Delta t = \frac{m_P C (T_{P_1} - T_{P_2})}{A_P \sigma \epsilon T_{AVG}^4} + \frac{1.31 L \Delta m_{CO_2}}{\sigma \epsilon A_P T_{AVG}^4} \tag{47}$$

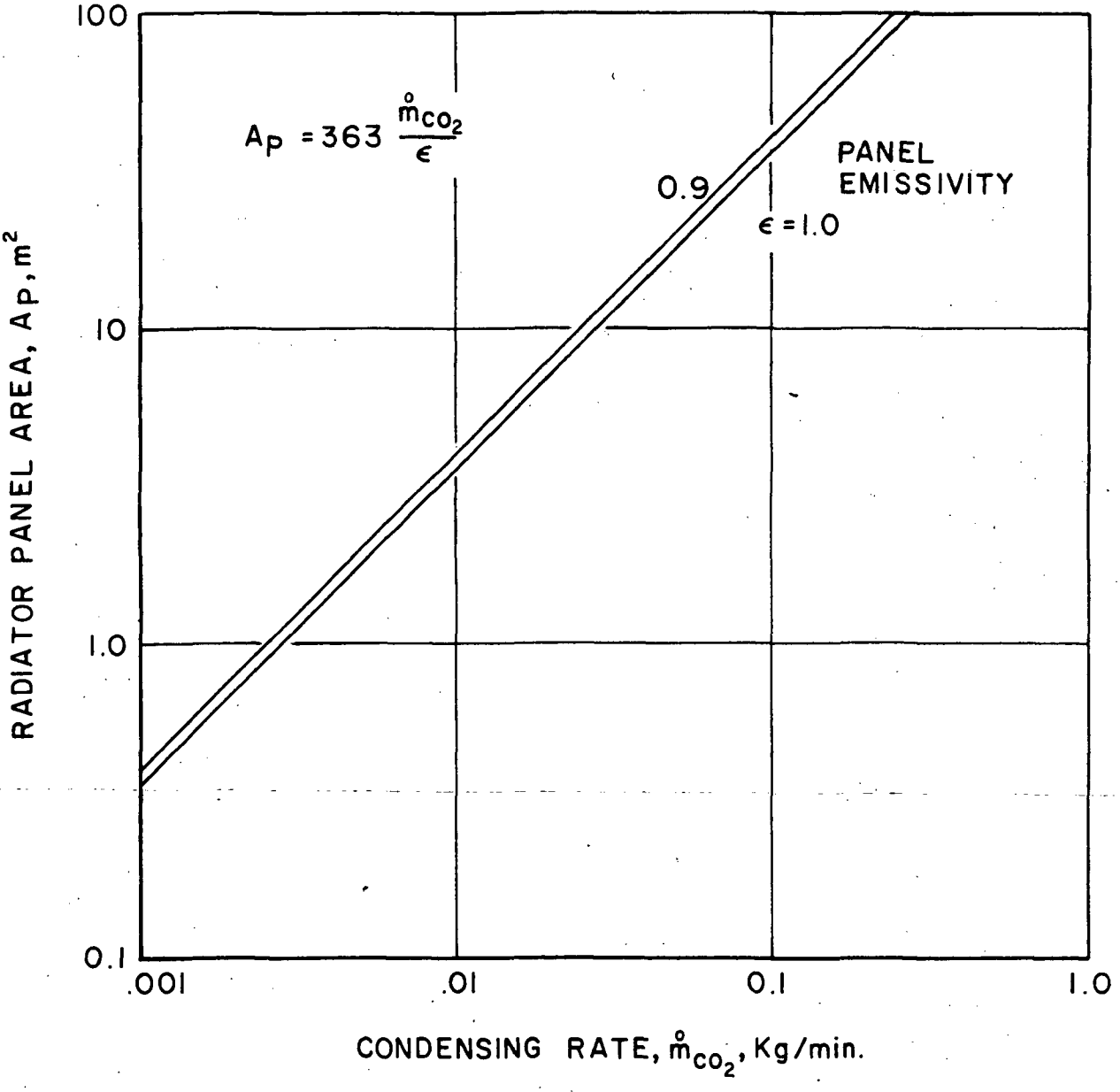

Figure 15.- Radiator panel area required to solidify CO_2.

For $\varepsilon = 0.9$ and aluminum, the time in minutes from $T_P = 190°K$ down to 162°K is:

$$\Delta t = 9.42 \frac{m_P}{A_P} + 265 \frac{\Delta m_{CO_2}}{A_P} \tag{48}$$

Figure 16 presents this dependence. For this phase of the cycle, increasing the panel area is beneficial in reducing the process time. However, the specific weight (first term) of 4.9 Kg/m^2 used introduces 46 minutes into the cycle for the radiator chilling.

During the cooling cycle, the resistance of the line from the molecular sieve to the thermal pump is of importance. A measure of this resistance is its reciprocal, conductance. Figure 17 displays the dependence of conductance on line diameter and length. For the CO_2 flow rates of interest, line flow is in the viscous regime. Also presented in figure 17 is the corresponding pressure drop for a typical mass flow rate of 0.5 Kg/hr. Relative to a nominal sieve desorb pressure of 0.034 atmospheres, pressure drop is negligible for lines with inside diameters of at least 2 centimeters.

The thermal radiated power removed during cooling is just

$$\dot{q} = \sigma \varepsilon A_P T_P^4 \tag{49}$$

and is plotted in figure 18. An integration of the overall cooling rate (heat from the desorbed CO_2 and Freon-21) of the thermal pump yields an average cooling rate of about 3 kilowatts for a typical radiator panel size of 10 square meters. It is this factor which could partly justify the addition of radiators to the spacecraft to effect thermal pumping of CO_2.

Thermodynamics of the Heating Cycle

Figure 19 presents a phase diagram for carbon dioxide and characterizes the thermodynamic events of the thermal pump. As a design objective, 0.034 atm (0.5 psia) was selected for the desorb pump level. This pressure corresponds to 162°K on the solid-vapor CO_2 equilibrium phase line, state 1 in the P-T plot of figure 19. After desorbing, the pump volume is isolated. Heating will drive the pressure up along the equilibrium line until the CO_2 is all vapor, point 2 in figure 19, for example. Subsequent heating will then follow a constant volume line ($P \sim T$) to the final temperature at a maximum pressure at point 4. It is convenient to consider the pump in this way to generalize the pumping capability relative to different storage tank pressures. Realistically, however, the pump would be connected through a check valve to a storage tank at some pressure at point 3. Continued heating would transfer the expanding CO_2 along the constant pressure line (dashed in figure 19) to the pressure at point 5. A slight pressure rise would occur from point 3 to point 5 depending on the actual volume of the storage tank.

PANEL UNIT MASS, $\frac{m_P}{A_P}$ = 4.9 Kg/m² (1.0 lb/ft²)

PANEL EMISSIVITY, ϵ = 0.9

$$\Delta t = 9.42 \frac{m_P}{A_P} + 265 \frac{\Delta m_{CO_2}}{A_P}$$

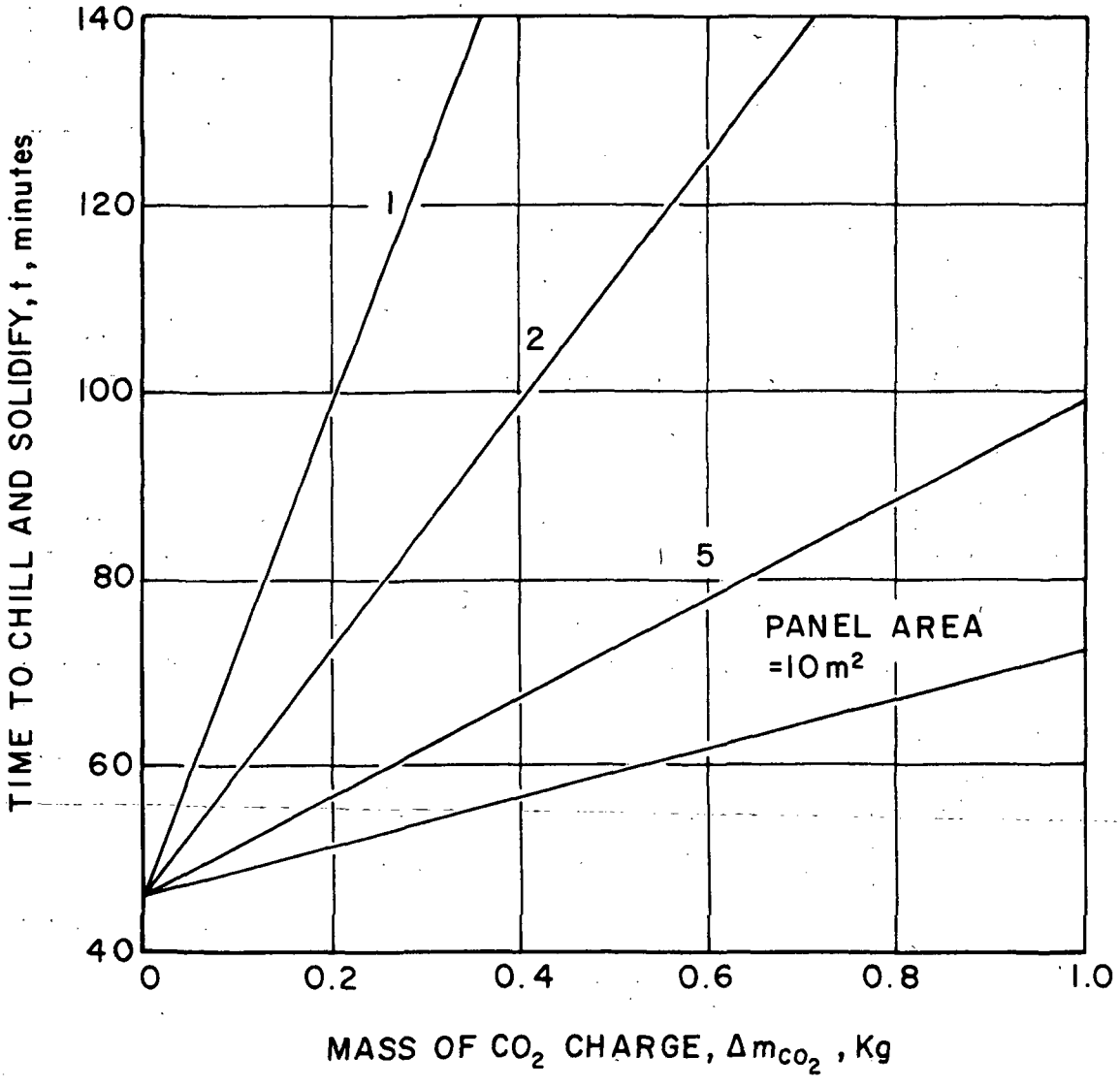

Figure 16.- Time to chill radiator from 190°K to 162°K and solidify CO_2.

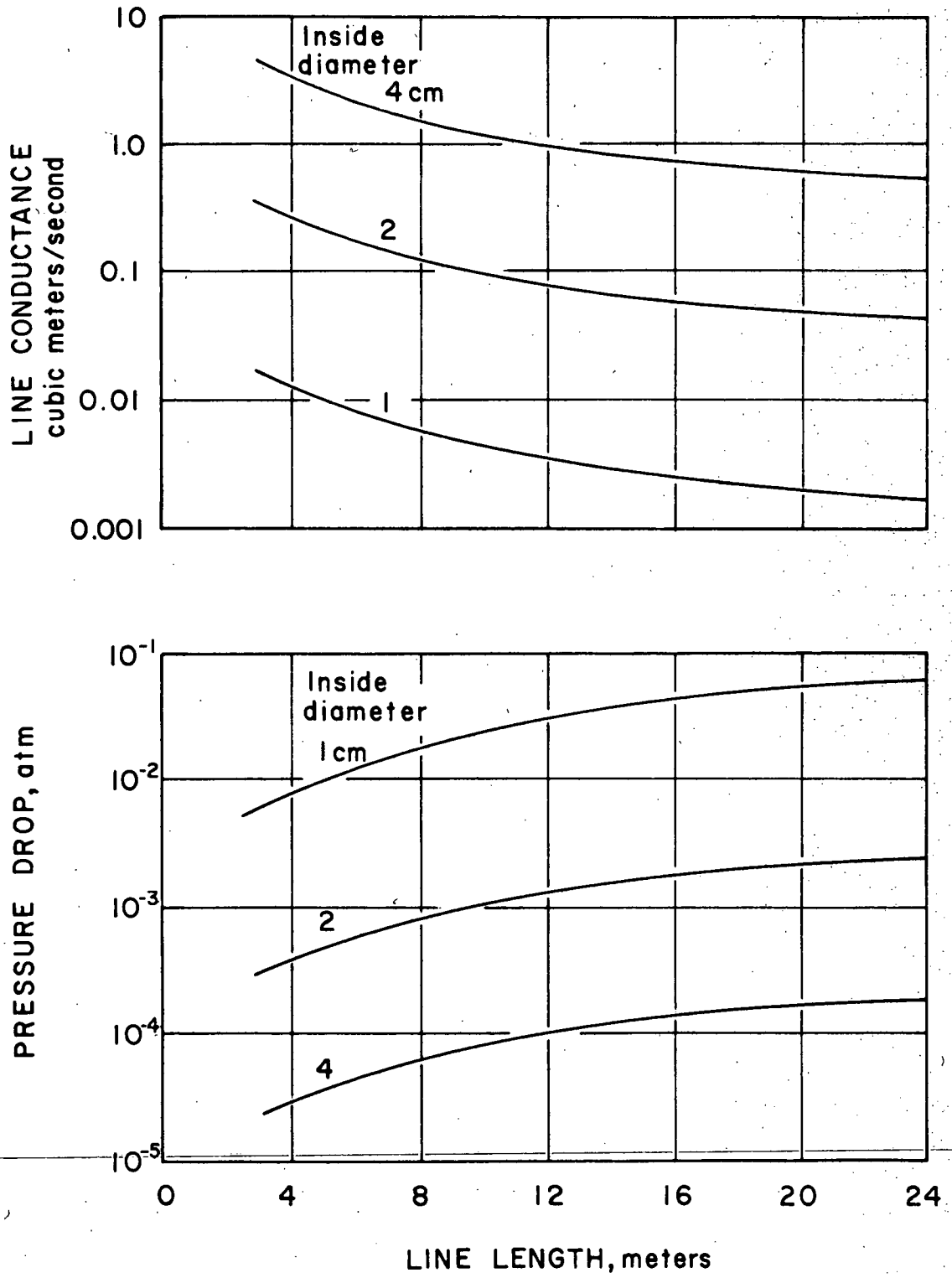

Figure 17.- Line conductance and pressure drop.

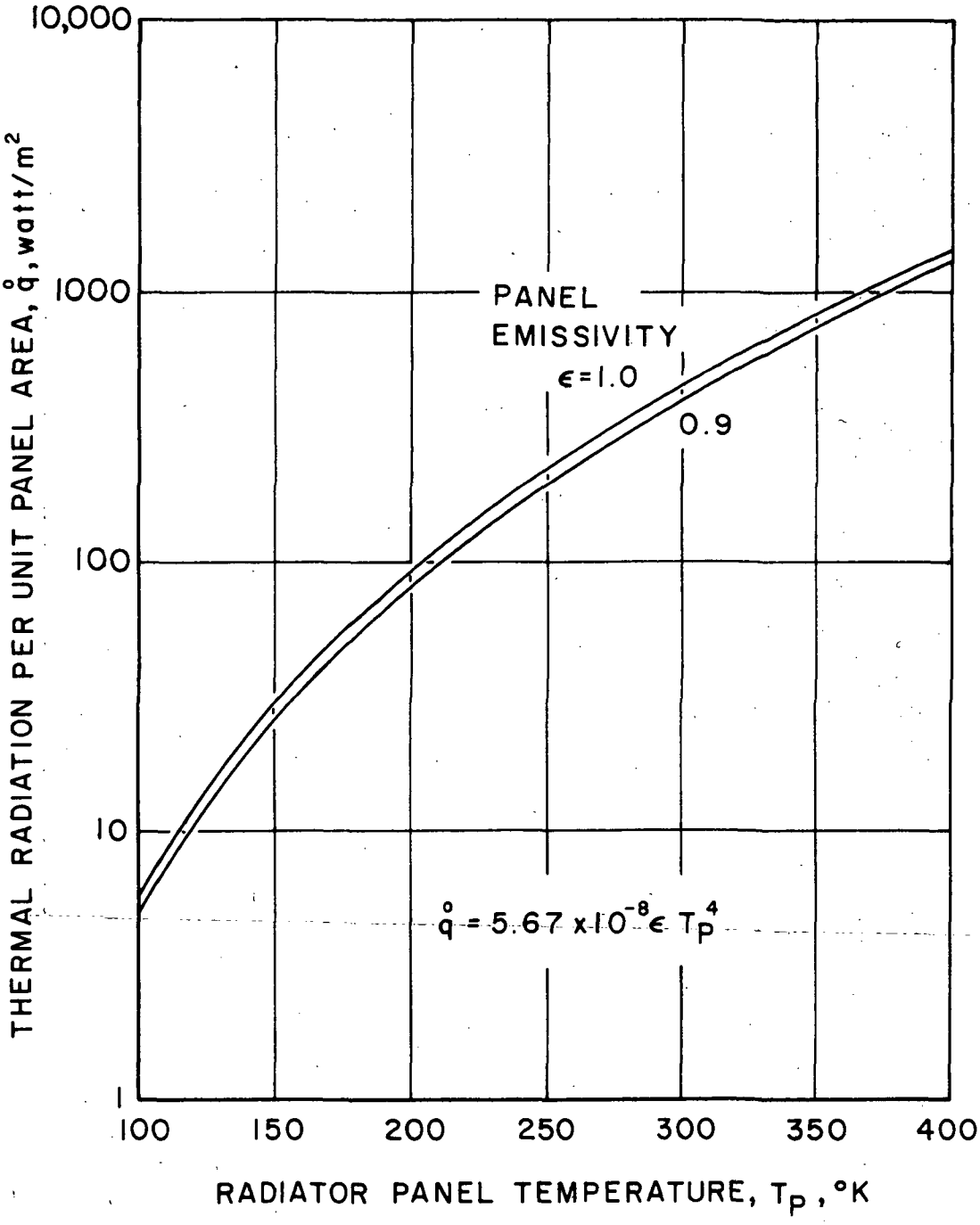

Figure 18.- Radiated power.

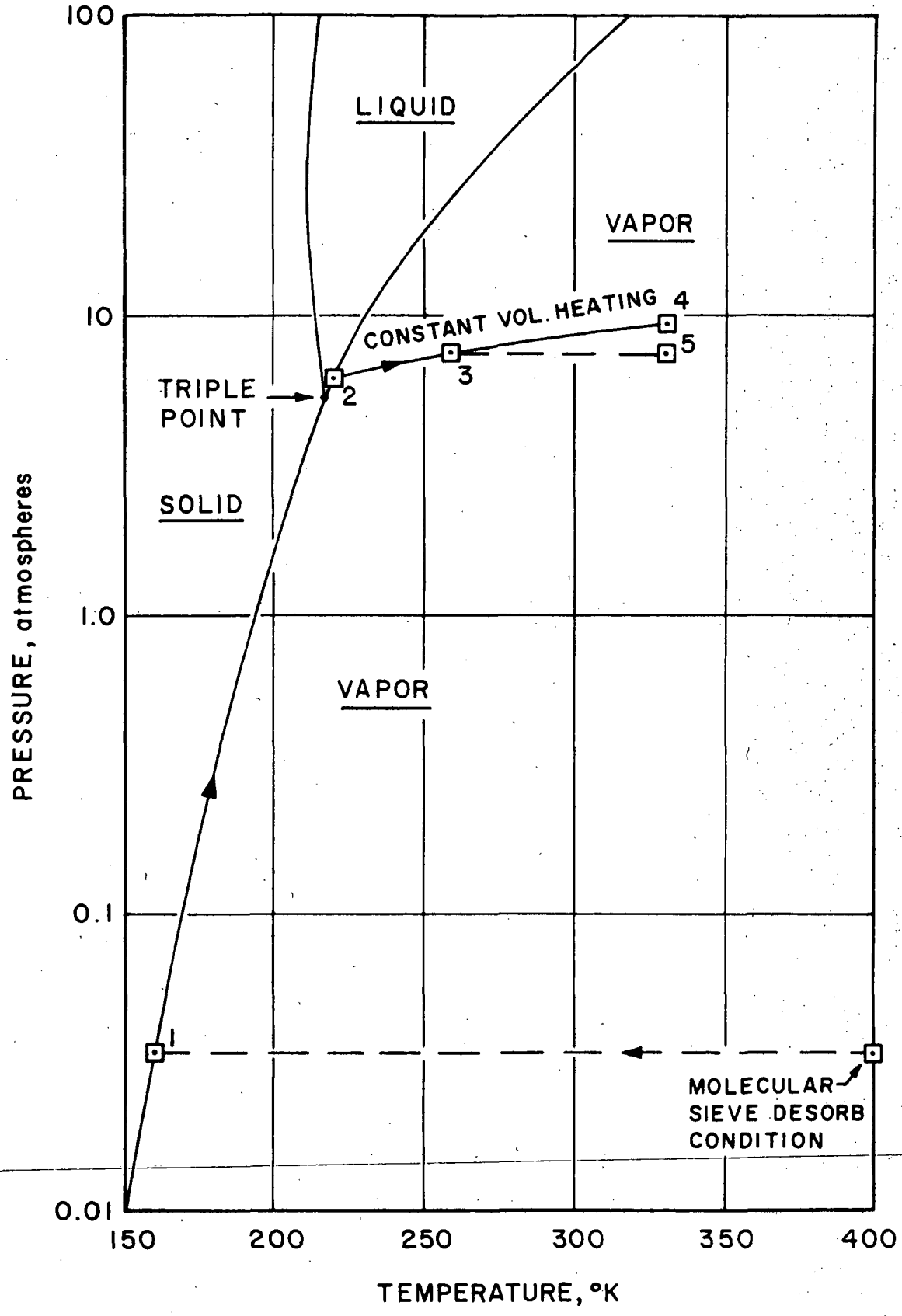

Figure 19.- Phase diagram characteristics of the thermal pump.

Heating is provided by Freon-21 circulating through the radiator. Freon-21 is liquid down to 138.5°K at atmospheric pressure, and will be available at temperatures up to about 330°K from the spacecraft heat rejection system. Although the panel surface radiating to space could be mechanically shuttered off during the heating phase, a simpler and lighter solution is to leave the panel radiator in a cooling mode, and provide sufficient heat transfer from the Freon-21.

The heat input from the Freon-21 goes to warming the metal radiator and the CO_2 and to the radiative cooling to space. The radiator is heated rapidly by the Freon with the CO_2 sensible and latent heating and the continued cooling to space second order factors. Therefore, it is sufficiently accurate to consider only the thermal capacity of the metal:

$$h\ (T_F - T_P)\ A_T = C\ \frac{dT_P}{dt} \left(\frac{m}{A}\right)_P\ A_P \tag{50}$$

A_T is the surface area of the Freon-21 heating tube in square meters and h is the convective heat transfer coefficient in watts/m^2-°K. Subscripts F, P and T are for Freon-21, panel, and tube, respectively. Solving (50) and integrating for the time to heat the radiator panel:

$$dt = \left(\frac{C}{h}\right)\left(\frac{m}{A}\right)_P \left(\frac{A_P}{A_T}\right) \frac{dT_P}{T_F - T_P} \tag{51}$$

$$t = \left(\frac{C}{h}\right)\left(\frac{m}{A}\right)_P \left(\frac{A_P}{A_T}\right) \ln \left(\frac{T_F - T_{P_1}}{T_F - T_{P_2}}\right) \tag{52}$$

The non-dimensional time values are displayed in figure 20 for a final panel temperature T_{P_2} of 300°K, and Freon-21 temperature T_F of 310°K.

As an example of the radiator panel heating time from 162°K to 300°K, read a value of the non-dimensional time of 2.7 from figure 20. Typical values of the parameters in equation (52) are:

$$C = 15.5\ \frac{\text{watt-minutes}}{\text{Kg-°K}} \qquad h = 2000\ \frac{\text{watts}}{m^2\text{-°K}}$$

$$\left(\frac{m}{A}\right)_P = 4.9\ \frac{Kg}{m^2} \qquad \frac{A_P}{A_T} = 20$$

The time to heat the radiator panel is about 2 minutes.

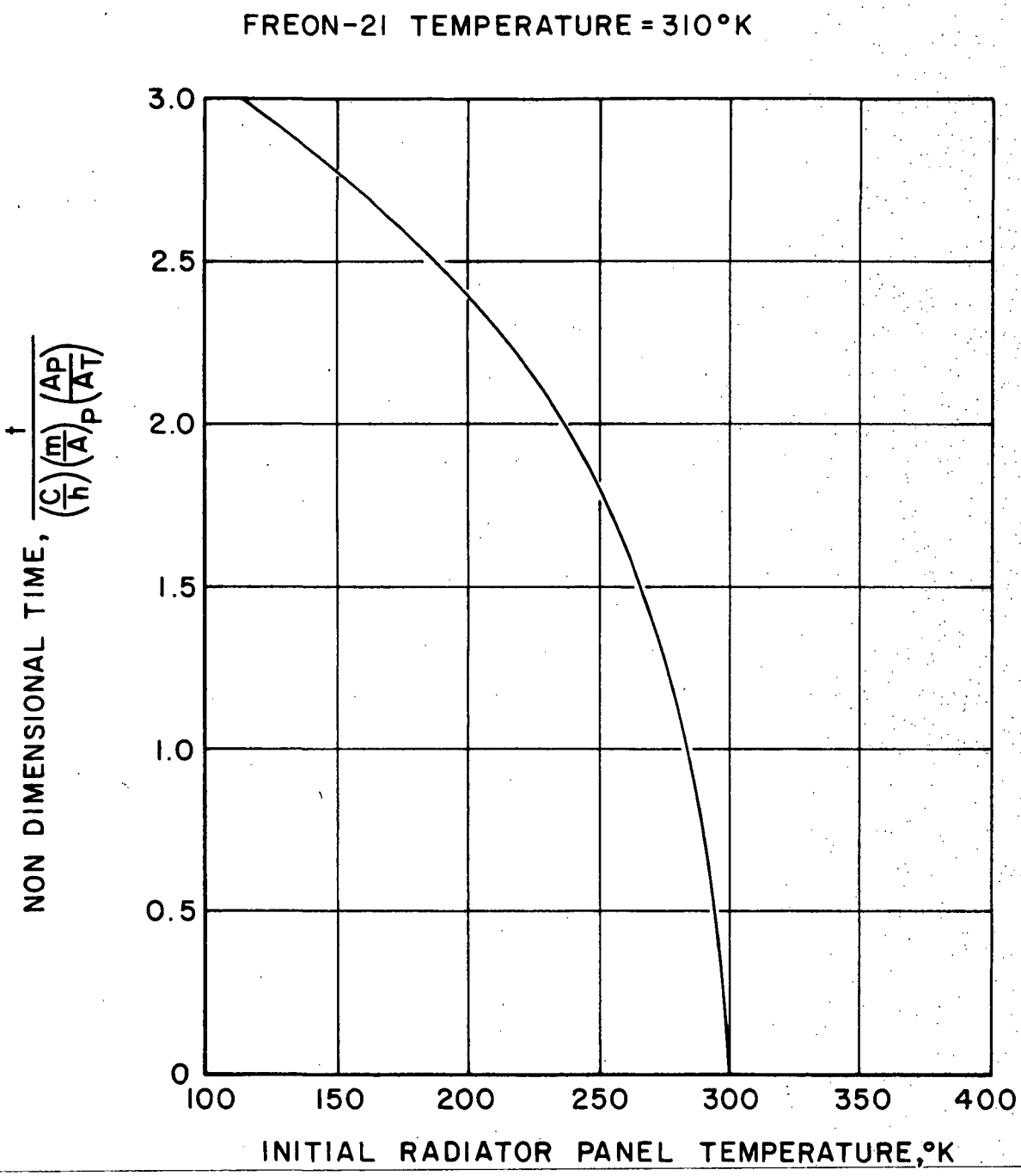

Figure 20.- Time to heat radiator panel.

Pump volume is a critical parameter for the pressurizing phase of the thermal pump cycle as well as for insuring that the dry ice does not clog the inlet regions and preclude additional solidification. The ratio of solid CO_2 volume to the total volume in the pump after it is isolated from the molecular sieve is called f_v.

The relationship between the volumes occupied by solid (or liquid) and vapor CO_2 can be derived as follows:

Define f_v = volume of solid/total volume. Since

$$m_{TOTAL} = m_{SOLID} + m_{VAPOR} = \rho_S f_v V + \rho_V (1 - f_v) V = \bar{\rho} V \tag{53}$$

where m is the mass in Kg, $\bar{\rho}$ is the average density in Kg/m^3, V is the total volume, and subscripts S and V are for solid and vapor phases. Solving,

$$\bar{\rho} = \rho_S f_v + \rho_V (1 - f_v) \tag{54}$$

Solving for the volume fraction, then

$$f_v = \frac{\bar{\rho} - \rho_V}{\rho_S - \rho_V} \tag{55}$$

Often the mass fraction is required. The analogous derivation is

$$V = V_S + V_V = \frac{f_m M}{\rho_S} + \frac{(1 - f_m) M}{\rho_V} = \frac{M}{\bar{\rho}} \tag{56}$$

where f_m is the mass of solid/total mass and M is the total mass. Solving,

$$\frac{1}{\bar{\rho}} = \frac{f_m}{\rho_S} + \frac{1 - f_m}{\rho_V} \tag{57}$$

Solving for the mass fraction,

$$f_m = \frac{\frac{1}{\rho_V} - \frac{1}{\bar{\rho}}}{\frac{1}{\rho_V} - \frac{1}{\rho_S}} \tag{58}$$

The volume and mass fractions are related by:

$$f_m = \frac{\rho_S}{\bar{\rho}} f_v \tag{59}$$

A typical calculation is presented to display the use of these parameters. Select $f_v = 0.01$. This means that as the heating phase starts, 1 percent of the pump volume is occupied by solid CO_2 at 162°K and 0.034 atm (0.5 psia). At that point on the solid-vapor equilibrium line, point 1 of figure 19, the solid and vapor densities are

$$\rho_S = 1608 \text{ Kg/m}^3 \qquad \rho_V = 0.11 \text{ Kg/m}^3$$

Thus

$$\bar{\rho} = 1608(0.01) + 0.11(0.99) = 16.19 \text{ Kg/m}^3$$

The mass fraction which is solid is very large:

$$f_m = \frac{\frac{1}{\rho_V} - \frac{1}{\bar{\rho}}}{\frac{1}{\rho_V} - \frac{1}{\rho_S}} \simeq 1 - \frac{\rho_V(\rho_S - \bar{\rho})}{\rho_S \bar{\rho}} \quad \text{as } \rho_V << \rho_S, \bar{\rho} \tag{60}$$

$$f_m = 1 - 0.00067 = 0.99933 \text{ for this case}$$

Heating now drives the pressure up the equilibrium line* in figure 19 until the CO_2 is all vapor. At this point 2,

$$\rho_{V_2} = \bar{\rho} = 16.19 \text{ Kg/m}^3$$

and

$$P_2 = 6.3 \text{ atm} \qquad T_2 = 220°\text{K}$$

*Note that for the case displayed, the triple point was passed in heating, and the liquid-vapor line followed to state 2. The volume fraction which corresponds to full vapor at the triple point is $f_v = 0.0086$.

Constant volume heating thereafter to $T_4 = 330°K$, for example, gives the final pressure at point 4

$$P_4 = 6.3\left(\frac{330}{220}\right) = 9.4 \text{ atm}$$

General results are plotted in figure 21 for one nominal value of final temperature T_4 equal to 300°K. The final pressure P_4 is simply proportional to the final temperature for other values.

The fraction of the CO_2 in the thermal pump volume which will be delivered to a receiver depends on the pressure in that receiver, P_5 in figure 19. Consider the mass (now all vapor) in the pump volume before

$$m_4 = \frac{P_4 V}{RT_4} \tag{61}$$

and after tripping a relief valve set at receiver pressure P_5

$$m_5 = \frac{P_5 V}{RT_5} \tag{62}$$

The fraction of the original mass delivered is then

$$\frac{m_4 - m_5}{m_4} = 1 - \frac{P_5}{P_4}\frac{T_4}{T_5} \tag{63}$$

The process will be between isothermal and adiabatic, probably closer to adiabatic. For $\gamma = 1.25$, the charge fraction pumped is

$$\frac{m_4 - m_5}{m_4} = 1 - \left(\frac{P_5}{P_4}\right)^{0.8} \tag{64}$$

The results are plotted in figure 22 for receiver pressures from 2 to 20 atmospheres. The dotted line in figure 19, point 3 to point 5, represents the process for a receiver pressure of 7.5 atm with the example presented following equation (59) for $f_v = 0.01$. Figures 21 and 22 are used to determine the amount of CO_2 actually pumped and, conversely, the amount of CO_2 which remains in the pump to be recycled.

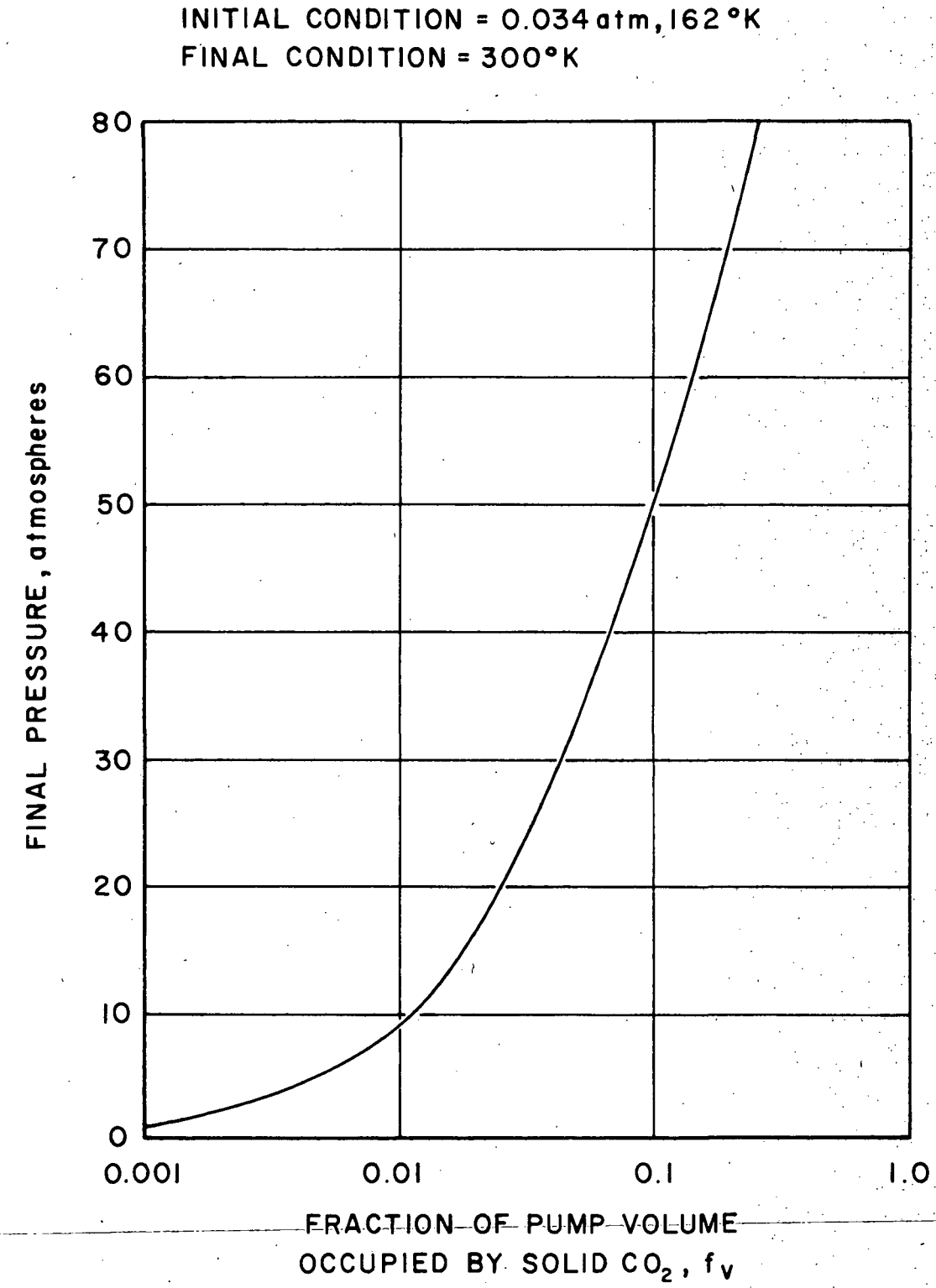

Figure 21.- Effect of volume ratio on pumped pressure.

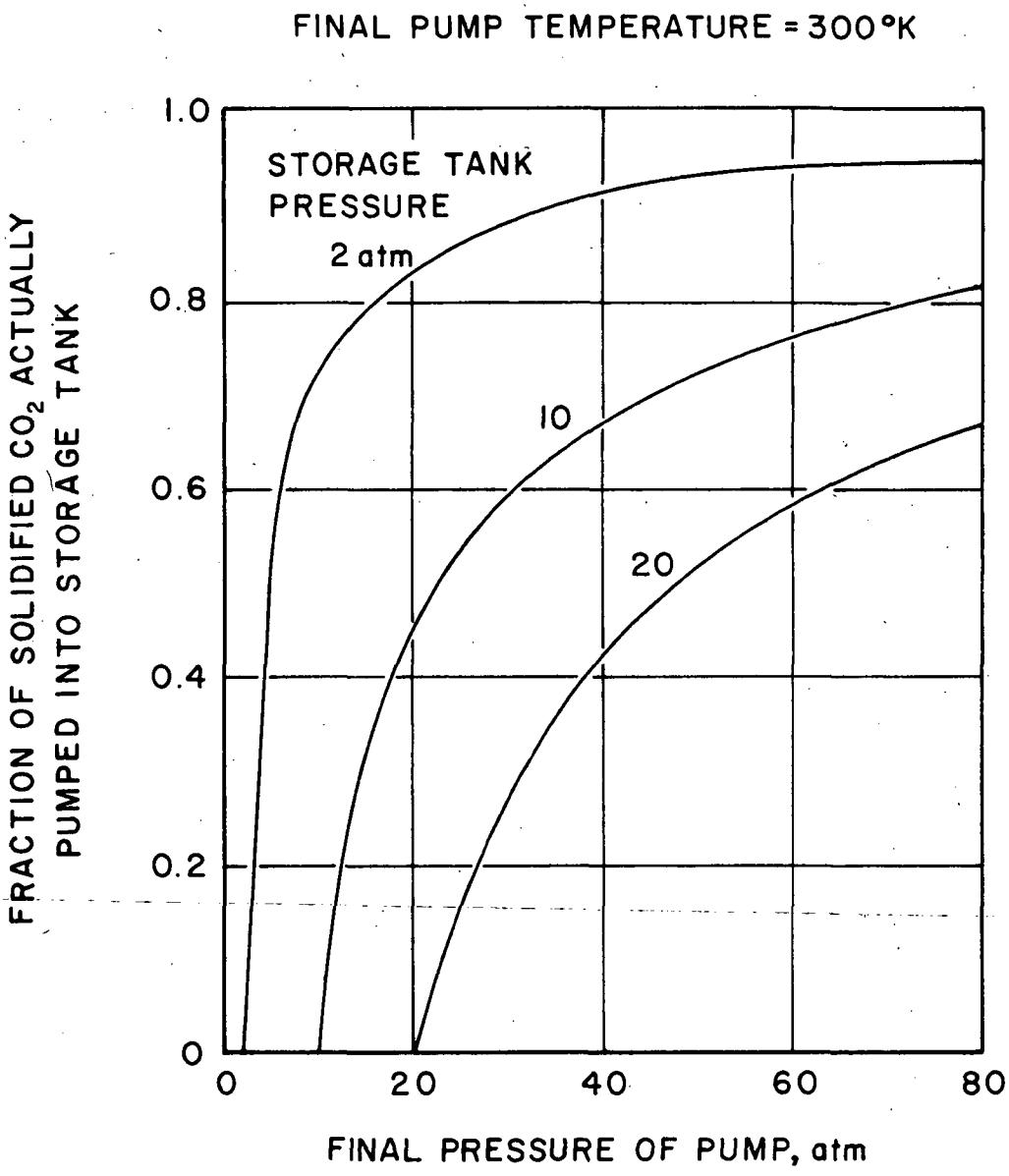

Figure 22.- Pumping effectiveness.

Effect of Non-condensables

Relative to the solidification of carbon dioxide down to 162°K, traces of O_2 and N_2, which can be considered non-condensables, are anticipated (ref. 11). Reference 12 describes the phenomenon in which cryotrapping can remove non-condensable gases by physically burying the gas in the cryotrapped condensate. The non-condensables, if untrapped, present a problem with the thermal pump due to added background pressure by virtue of their partial pressures. If the non-condensables are effectively trapped, then the problem is solved and the non-condensables pass on with the CO_2 during the heating/pumping cycle. It is likely that partial cryotrapping will occur and lessen the non-condensable problem; however, the degree of cryotrapping is not known at this time. As a conservative estimate of the effect of non-condensables on the thermal pump, the limiting case of zero cryotrapping will be considered here.

A convenient representation of the effects of non-condensables can be derived using the solid CO_2 volume ratio f_v and a non-condensable mass ratio λ, where

$$f_v = \frac{\text{volume of solid } CO_2}{\text{total volume}}$$

$$\lambda = \frac{\text{mass of non-condensables}}{\text{total mass}}$$

An expression for the percentage of CO_2 vapor pressure can be derived in terms of the above parameters. The derivation is lengthy and will not be given here, however. An exact expression for the CO_2 vapor pressure is:

$$\frac{P_{CO_2}}{P_T} = \frac{1 - \left(\frac{\lambda}{1-\lambda}\right)\left(\frac{f_v}{1-f_v}\right)\left(\frac{\rho_S}{\rho_{NC}}\right)}{1 + \left(\frac{\lambda}{1-\lambda}\right)\left(\frac{\rho_V}{\rho_{NC}}\right)} \tag{65}$$

where P_T is the total vapor-gas pressure. Using typical values of the solid, vapor and non-condensable densities, equation (65) becomes

$$\frac{P_{CO_2}}{P_T} = \frac{1 - \left(\frac{\lambda}{1-\lambda}\right)\left(\frac{f_v}{1-f_v}\right) 22{,}200}{1 + \frac{1.52\,\lambda}{1-\lambda}} \tag{66}$$

f_v and λ are both much less than one, permitting the following approximation

$$\frac{P_{CO_2}}{P_T} \simeq 1 - (22{,}200)\ \lambda f_v \qquad (67)$$

Figure 23 presents the permissible non-condensable mass ratio λ for levels of CO_2 volume ratio f_v relative to the acceptable values of non-condensable partial pressure. The limit line for all non-condensables (no CO_2) is given from the exact equation (65) and is academic. A reasonable partial pressure of non-condensables would be about 10 percent, for example. Too high a non-condensable pressure would offer back pressure resistance to the sieve and would require higher sieve pressures or, conversely, lower pump temperatures. For 10 percent non-condensables and a desired solid CO_2 volume ratio of 0.01, as an example, figure 23 indicates that non-condensables can reach a mass ratio λ of 4×10^{-4}. Values projected in reference 11, however, indicate an $O_2 + N_2$ mass ratio of about 10^{-2}. Unless cryotrapping is very effective, the non-condensables would have to be vented out of the thermal pump at intervals to maintain λ at or below the 4×10^{-4} value.

Venting would be simple, involving a momentary venting to space vacuum. Losses due to such venting have not been analyzed but should be small (of the order of a few percent). An advantageous effect of the venting would be to decrease the amount of oxygen contained in the biowaste resistojet propellant which would permit higher operating temperatures with the current resistojet design (ref. 13).

Overall Cycle Time

The overall cycle time to pump CO_2 from the molecular sieves at 0.034 atm to the storage tanks at 2 to 20 atm is found to be reasonable. The first term in equation (48) reflects a predominate radiator cool-down term following the heating/pumping portion of the cycle. It was pointed out that the chill time is independent of radiator size. For a realistic radiator mass to area ratio of 4.9 Kg/m^2, 54 minutes are required for chilling the radiator from 300 to 190°K (fig. 14) plus 46 minutes, reflected by the starting point for the curves in figure 16, to chill from 190 to 162°K. On the other hand, the heating time is insignificant at about 2 minutes, as shown in the example evaluated for equation (52).

The molecular sieves desorb every 30 minutes. However, a 30-minute pumping cycle is not possible with the 100-minute chill time. Unless the radiator mass-to-area ratio can be reduced to about one Kg/m^2 or less, the pump cycle time will exceed 30 minutes. To effect pumping, then, several sieve desorbs must be condensed into the pump in order to amortize the radiator chill time.

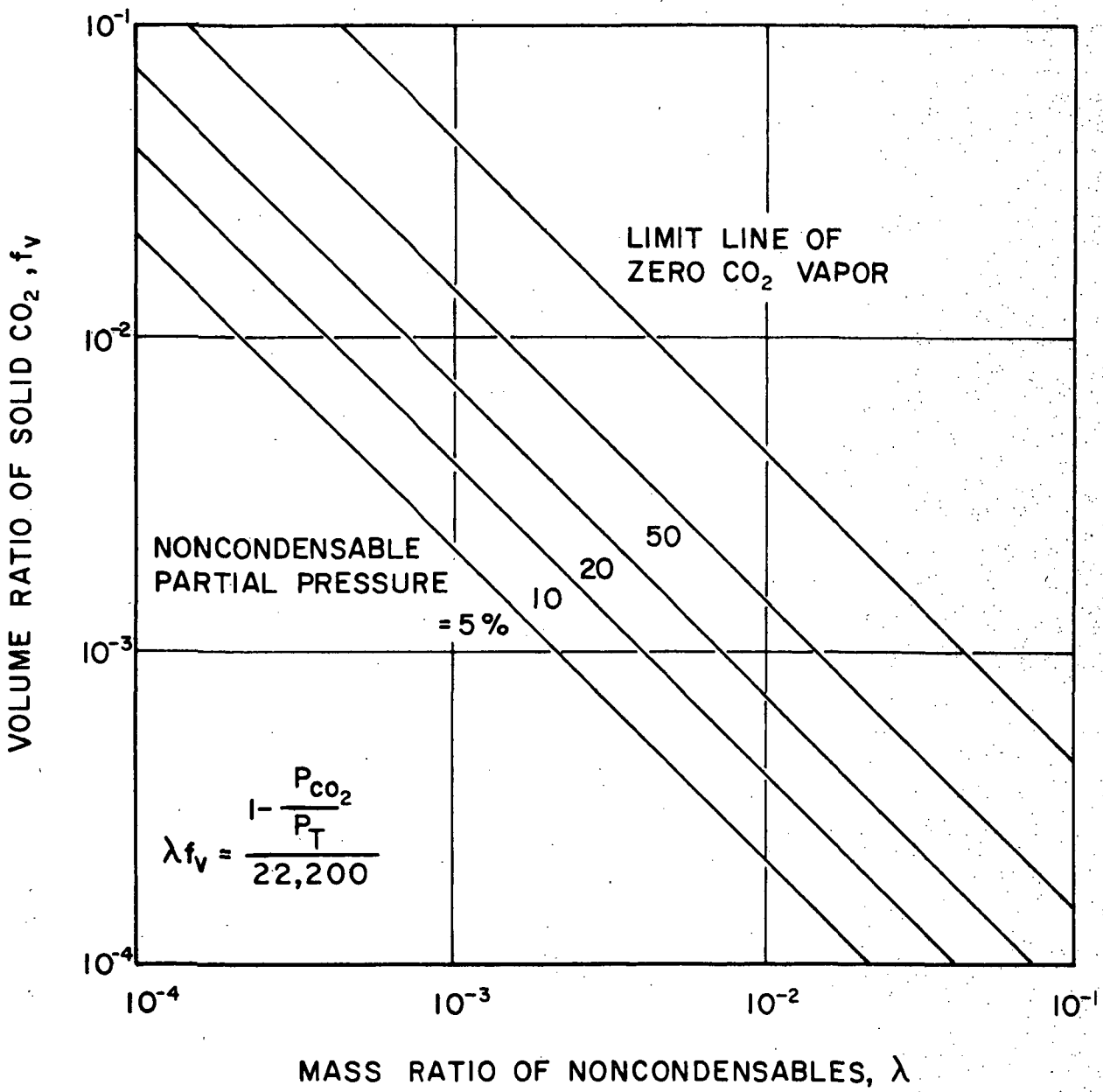

Figure 23.- Effect of non-condensables on CO_2 solid volume ratio.

Two typical example cases will be examined here to show thermal pump feasibility relative to cycle time.

Case I - Assume a storage tank pressure P_5 of 2 atm and a solid CO_2 volume ratio f_v of 0.01 for which the non-condensable problem is not severe. From figure 21, the hypothetical P_4 is found to be 9.3 atm. From figure 22, the fraction pumped is 72 percent. This means that 28 percent of the CO_2 accumulated in the pump must be recycled. To pump 0.5 Kg/hr, it is then necessary to condense 0.5/0.72 or 0.695 Kg/hr, equal to 0.0116 Kg/min. From figure 14, the chill to 190°K is 54 minutes. From figure 15, we see that a radiator area of 4.5 m^2 (ε = 0.9) will handle the solidification of the CO_2. Additional panel area will be needed to handle the chill time and effect a reasonable overall cycle time. Assume twice the above area or about 10 m^2. The overall cycle time is obtained from figure 16 by iteration. Assume a cycle time t_C. Obtain the CO_2 charge mass as 0.0116 t_C. Find the time to chill the radiator and solidify the CO_2 from figure 16. Add 2 minutes (reheat time) and the above 54 minutes to this value to get the t_C required. A solution is obtained when the required t_C equals the assumed t_C. For the above parameters, we find the overall cycle time to be 150 minutes.

Case II - Assume a storage tank pressure P_5 of 20 atm and a solid CO_2 volume ratio of 0.1. The value of f_v of 0.1 (higher than for Case I) is dictated by figures 21 and 22 in order to have a reasonable (low) recycled amount of CO_2. If too much CO_2 is recycled, overall cycle times can become prohibitively long. As before, from figure 21, find P_4 equal to 52 atm. The fraction pumped is now 53 percent from figure 22. Therefore, to pump 0.5 Kg/hr, we need to condense 0.5/0.53 or 0.943 Kg/hr or 0.0157 Kg/min. The chill to 190°K is again 54 minutes. Figure 15 indicates 6.2 m^2 of radiator area are sufficient for CO_2 solidification. Again, use 10 m^2 to cover the heating requirement. From an iteration around figure 16, the overall cycle time is found to be 175 minutes. Non-condensables, if not cryotrapped to a significant degree, become a problem with an f_v of 0.1 as seen in figure 23. Frequent ventings would be required to maintain a reasonable partial pressure of non-condensables.

Case II, to pump to a 20 atmosphere storage tank pressure, requires a higher value of the volume ratio f_v of 0.1 compared to Case I (f_v equal to 0.01). Gas-side volume is larger for the Case I situation. For 10 m^2 of radiator surface, the pump would consist typically of panels about 0.2 meter wide with a total length of about 50 meters. The total volumes of the CO_2 gas-side space would be about 0.05 and 0.008 m^3, respectively, for the Case I and II situations. Respective gas side tube diameters would be about 4 and 1.5 cm with length to diameter ratios of about 1300 and 3500. Some manifolding would be possible to reduce the L/D of the gas side tubes. Manifolding would be limited, however, since the

condensing space would become smaller in cross section as manifold volume was added. It does appear that a CO_2 blockage problem from local condensation will occur.

The thermal pump cycle has not been examined for the effects of space station orientation relative to the sun. The radiator will not be able to condense CO_2 when in a direct sunny-side exposure. The 150 and 175 minute cycle times calculated as examples above may not be compatible with some space station orientations. In any case, more than one pump would be required to have always available a dark side exposure. The purpose of this study is to determine feasibility of the cycle. The cycle appears to be thermodynamically feasible if cycle times up to about 200 minutes are, subsequently, feasible with spacecraft orientation relative to the sun.

The thermal pump is considered heavy (for example, 10 m^2 at 4.9 Kg/m^2 equates to about 50 Kg or 100 lb) relative to mechanical pumps. This factor is compensated, however, by the advantages of not requiring electrical power (other than small solenoid power consumption) and by supplementing or replacing part of the space station waste heat radiator system. The pump has been shown to be able to handle a 20 atmosphere storage tank pressure requirement in a not too unreasonable cycle time of less than 200 minutes. The cycle time and weight can be reduced considerably with a lower radiator mass to area ratio. A realistic specific mass of 4.9 Kg/m^2 has been used in the above evaluation, however, and significant improvements in this direction are not likely.

CONCLUSIONS

Mass Flow Limiters

A dozen techniques were considered which could provide flow limiting of liquid water propellant to the biowaste resistojet. Flow limiting relative to an unrestricted - constant pressure supply is required to prevent thermal quenching of the thrustor, erratic thrusting performance, and the formation of ice crystals in the thrustor nozzle. A pre-evaporator can provide the necessary flow stability during start-up transients of the thrustor provided the evaporator is sufficiently large and has adequate thermal capacity. The evaporator must be preheated to a ready-to-steam condition to provide sufficient flow stability. A more effective flow limiting device can provide the following improvements in the propellant-thrustor system:

1. Shorten the start-up transient.
2. Permit a smaller, lighter evaporator.
3. Improve the system reliability against adverse start-up conditions.
4. Reduce the sensitivity of thrust to changes in the propellant supply pressure.

A numerical example is given for item 4 in the technical discussion. It shows that supply pressure allowable tolerance limits can be broadened by about 30% with a flow restrictor without incurring an additional thrust error.

Of the many candidate flow limiter concepts, the following were selected for further study on the basis of high reliability:

1. Contraction - expansion type flow restrictor (orifice or nozzle).
2. Cavitating venturi nozzle.
3. Unvented vortex valve.
4. Hybrid type flow limiter.
5. Laminar conduit flow restrictor.
6. Turbulent conduit flow restrictor.

The first four items were studied experimentally after it was determined analytically that there is no advantage in using the laminar and turbulent conduit devices compared to the contraction-expansion device. In the small flow sizes which are compatible with the biowaste resistojet, cavitation was not self-induced in the venturis and ultrasonic excitation was employed. While not conclusive because only three typical venturis were tested, the ultrasonic excitation did not induce sufficient cavitation to result in flow limiting. Instead, flow rates tended to increase about 2% for a given pressure differential when excitation was applied, apparently due to a reduction of the viscous boundary effects.

The vortex valve demonstrated better flow limiting than a contraction-expansion device at high flow rates. When scaled down to biowaste resistojet flow rates, the reverse was true. These results should be qualified in that the vortex valve was not optimized for the lowest flow rates. Indications are, however, that even if properly scaled, the vortex valve would not be significantly better than a simple orifice for flow limiting.

A simple hybrid flow limiter was conceived and tested; it exhibited excellent flow limiting performance. This device consists of a stiff metal diaphragm which moves under pressure differential loading to close one of two holes in a nearby orifice plate. A bypass hole is provided in the diaphragm which is in series with the orifice plate holes. At the initial thrustor start-up condition, the pressure differential is greatest and the diaphragm closes one orifice plate hole. As thrustor pressure increases, the pressure differential decreases and the diaphragm relaxes to increase the flow area. The effect is to compensate the pressure differential reduction by increasing flow area to achieve a near constant mass flow rate.

The start-up dynamics of the thrustor are such that it is not necessarily desirable to have a perfect (constant mass flow rate) limiter. A

slightly higher initial mass flow rate helps build thrustor pressure up faster. Too high an initial flow may, on the other hand, increase the thermal response time. The hybrid flow limiter can be adjusted to provide an optimum flow limiting characteristic to match a specific propellant-thrustor system application.

Sensivitity of mass flow rate to pressure differential was used to compare the effectiveness of the various flow limiters. In the low mass flow rates of interest (a 25-mlb size biowaste resistojet is typical), the contraction-expansion device demonstrated a sensitivity (see equation 18) of about 0.7 as compared to a theoretical value of 0.5. The higher 0.7 value is the result of viscous effects becoming predominate at the low flow rates of interest. For the same flow conditions, the hybrid flow limiter demonstrated a sensitivity of 0.2. This is a considerable improvement over the contraction-expansion device. The hybrid device is inherently reliable. Stress levels in the hybrid device diaphragm are very low and are compatible with millions of cycles for corrosion resistant steel.

For applications of the resistojet using liquid water as a propellant, either the hybrid device or the contraction-expansion device (orifice or nozzle) can be recommended for propellant flow limiting. Either of these devices can be used effectively with a pre-evaporator or an integrated evaporator stage to optimize the start-up transient response of the resistojet, to prevent thrust instabilities, and to maximize the effective specific impulse of the thrustor.

Thermal Pumps

A typical biowaste propulsion system pumping requirement, that of pumping desorbed CO_2 from the molecular sieve to storage tanks at 2 to 20 atmospheres pressure, has been evaluated. The thermal pump concept, using cryopumping in space radiators with waste heat to raise the pressure of solidified CO_2, appears feasible with one possible exception. The requirement for a small cryopump gas-side volume relative to large space radiator areas involves a gas-side space long and slender which would be susceptible to local blockage by solidifying CO_2.

Another factor which may present difficulties is the cycle time of the thermal pump. A realistic radiator specific weight of 4.9 Kg/m^2 (1.0 lb/ft^2) results in a 100 minute time to chill the radiator, after heating, to begin a new solidification cycle. The expected molecular sieve desorb cycle is 30 minutes. The thermal pump must be operated in a 150 to 175 minute cycle which may, under certain space station orientations, involve a conflict with dark side-sun side exposures. Unless a significantly lower specific weight is possible to shorten the radiator chill time, it then may be necessary to use several thermal pumps at about 50 Kg or about 100 pounds mass per pump. When thermal pumps are not being used to pump CO_2, they can be used as waste heat radiators. In effect, the thermal pump is nothing more than modified waste heat radiator already proposed for the space station.

Advantages of the thermal pump concept include elimination of the electrical power consumption of the baseline mechanical pumps, and possible removal of oxygen trace gas which would benefit the metal heater type resistojet thrustor. This latter factor may actually involve a trade-off, higher specific impulse with the resistojet not having to handle oxygen versus more propellant if the oxygen is not vented from the thermal pump. An advanced biowaste resistojet using ceramic heater elements is under development (ref. 14) which is not affected by oxygen in the basic biowaste propellants. The size and weight of the thermal pump are compensated by its capacity for dumping waste heat and thereby supplementing or replacing part of the spacecraft radiator.

The thermal pump is essentially a space radiator structure which would normally be integral with and serve as space station structure and meteor shielding. Final practicality and feasibility must include the judgment of the space station structural designer. In addition, other pumping situations, not necessarily related to the resistojet propulsion system, may adapt to the thermal pump concept. This report presents a preliminary design method using the CO_2 for resistojet propulsion as an example. It is recommended that further consideration by EC/LS study groups be made of the thermal pump concept.

REFERENCES

1. Halbach, C.R.: Technology Development of a Biowaste Resistojet. First Quarterly Report, Marquardt Co. Report 25203, December 1969.

2. Schreib, R.R.; Pugmire, T.K.; and Chapin, S.G.: The Hybrid (Hydrazine) Resistojet. Paper No. 69-496, presented at the AIAA 5th Propulsion Joint Specialist Conference, U.S. Air Force Academy, Colorado, June 9-13, 1969.

3. Halbach, C.R.: 10-mlb Biowaste Resistojet Performance. Paper No. 71-687, presented at the AIAA/SAE 7th Propulsion Joint Specialist Conference, Salt Lake City, Utah, June 14-18, 1971.

4. Pugmire, T.K.; et al.: Electrothermal Hydrazine Engine Performance. Paper No. 71-760, presented at the AIAA/SAE 7th Propulsion Joint Specialist Conference, Salt Lake City, Utah, June 14-18, 1971.

5. Knapp, R.T.: Cavitation Scale Effects. Proc. Seventh General Meeting IAHR, Lisbon, vol. I, paper A-6, 1957.

6. Oshima, R.: Theory of Scale Effects on Cavitation Inception on Axially Symmetric Bodies. Trans. ASME, 83, Ser. D., J. Basic Engr., p. 379-384, 1961.

7. Kermeen, R.W.; McGraw, J.T.; and Parkin, B.R.: Mechanism of Cavitation Inception and the Related Scale-effects Problem. Trans. ASME, 77 (4), p. 533-540, 1955.

8. Streeter, V.L. (Editor): Handbook of Fluid Dynamics. First Edition, McGraw-Hill, p. 12-13, 1961.

9. Halbach, C.R.: Technology Development of a Biowaste Resistojet, Sixth Quarterly Report, The Marquardt Co. Report S-998, March 1971.

10. Roark, R.J.: Formulas for Stress and Strain. Third Edition, McGraw-Hill, Chapter 10, 1954.

11. Greco, R.V.; and Bliss, J.R.: Resistojet Systems Studies Directed to the Space Station/Space Base, Volume I, Station/Base Biowaste Resistojet System Design, NASA CR-111879, McDonnell Douglas Report G2125, April 1971.

12. Anon: Basic Mechanisms of Noncondensable Gas Cryotrapping. General Technology Corporation Technical Documentary Report No. AEDC-TDR-63-147, July 1963.

13. Halbach, C.R.: Technology Development of a Biowaste Resistojet. Fourth Quarterly Report, The Marquardt Co. Report 25,313, Sept. 1970.

14. Halbach, C.R.; Page, R.J.; and Short, R.A.: High Temperature Biowaste Resistojets Using Electrically Conducting Ceramic Heaters. Preprint 72-454 presented at the AIAA 9th Electric Propulsion Conference, Bethesda, Maryland, April 17-19, 1972.